energies

MDPI

*Article*

# Design and Implementation of Finite-Time Convergent Adaptive ADRC for the Resilient Control of Power Converters

**Ghulam Shabbir [1], Ali Hasan [2,*], Muhammad Yaqoob Javed [3], Aamer Bilal Asghar [3] and Thomas Mussenbrock [2]**

[1] Department of Intelligent Systems, The University of Lahore, 1-KM Defense Road, Lahore 54792, Pakistan; engrshabbirr@gmail.com
[2] Faculty of Electrical Engineering and Information Technology, Ruhr University Bochum, 44780 Bochum, Germany; mussenbrock@aept.ruhr-uni-bochum.de
[3] Department of Electrical and Computer Engineering, COMSATS University Islamabad (CUI), Lahore Campus, Lahore 54000, Pakistan; yaqoob.javed@cuilahore.edu.pk (M.Y.J.); aamerbilal@cuilahore.edu.pk (A.B.A.)
* Correspondence: hasan@aept.ruhr-uni-bochum.de

**Abstract**

The dynamics of power converters are highly influenced by uncertainties, nonlinearities, and external disturbances. Thus, high-performance, extremely resilient, and robust control strategies are necessary for their control. For the robust operation of power converters, this article presents an adaptive and finite-time convergent active disturbance rejection control (ADRC) framework inspired by Professor Han's seminal paper. Based on ADRC's philosophy, this article proposes a control scheme that integrates adaptiveness and finite-time convergence in both the extended state observer and the control law. The proposed framework ensures quick disturbance estimation and its rejection, thus ensuring that the required response is tracked successfully. The controllers for different power converters, such as buck converters, boost converters, and single-phase inverters, are designed to ensure the desired dynamics, including low settling times and zero-percent overshoots. The controllers are implemented in the discrete-time domain using forward differences. Simscape simulation experiments on buck converters, boost converters, and single-phase inverters demonstrate that the responses are achieved with finite settling time with no overshoots. Thus, such control strategies are highly crucial for mission-critical power applications.

**Keywords:** active disturbance rejection control (ADRC); tracking differentiator (TD); adaptive extended state observer (AESO); finite-time convergent control (FTCL); buck converter; boost converter; single-phase inverter; three-phase inverter

Check for updates

Academic Editor: Pavlos S. Georgilakis

Received: 18 January 2026
Revised: 3 March 2026
Accepted: 19 March 2026
Published: 27 March 2026

**Copyright:** © 2026 by the authors. Licensee MDPI, Basel, Switzerland. This article is an open access article distributed under the terms and conditions of the Creative Commons Attribution (CC BY) license.

## 1. Introduction

Power electronic converters are the pillar of current energy systems, serving as vital interfaces between sources and loads in applications ranging from sustainable energy integration and microgrids to manufacturing industry and mission-critical structures. The operation of these converters is inherently influenced by uncertainties, nonlinearities, and external disturbances such as abrupt load changes, grid faults, electromagnetic interference, and component degradation. Resilient control becomes an unavoidable need to counteract such challenging environments. The resilient controller must meet the objectives of system stability, operational reliability, and desired dynamics under any kind of adverse conditions.

Conventional approaches for the control of converters have largely been based on linear techniques such as proportional–integral (PI) and proportional–resonant (PR) con-

trollers. Under moderately changing conditions, linear controllers are attractive because they can be designed and implemented using well-established linear mathematics. But their efficacy vanishes if they encounter nonlinear dynamics, parameter variations, or unmodelled dynamics [1]. These issues have somewhat been resolved using advanced linear techniques such as H-infinity control, internal model control, and model-predictive control, but their design and implementation require highly precise models. In the nonlinear domain, sliding-mode control (SMC) and its different variants based on variable control structures have been widely used. But these methods suffer from chattering and parameter variations [2].

ADRC, established by Professor Han, symbolizes a paradigm shift in control philosophy since it eliminates the need for a plant model to a huge extent. Instead of relying on the exact plant's model, it models the plant's dynamics using an $n$th-ordered integrator and an extra state called 'extended state'. This extended state representing all anomalies of the system is estimated using an extended state observer. Since these capabilities of ADRC give full control to the designer, they have made ADRC prominent as a resilient control framework [3].

Classical ADRC counts on the asymptotic convergence of ESO and the control law. Fixed asymptotic convergence might not be sufficient in highly time-varying dynamics. This limitation can be conquered by embedding adaptive and finite-time convergence into ESO and the control law. By instituting nonlinear error dynamics through $fal$-function-based structures, both the ESO and the control law can be tuned to drive estimation and tracking errors to zero within a finite horizon. This guarantees rapid revival from disturbances and improves reliability in mission-critical applications where delays in convergence can worsen system integrity [4].

Simscape simulation experiments on buck converters, boost converters, and single-phase inverters, operating roughly at 7.5 kW, underline the advantages of this approach. For the buck converter, the controller is designed to approximately achieve a convergence time of 250 μs, but the actual settling of 1 ms is achieved with the advantage of having zero-percent overshoot. The boost converter's control is designed to achieve a settling of 16 ms, obtaining approximately 22 ms of settling time with no overshoot in the final response. The controller for the single-phase inverter is designed for a settling time of 50 ms, achieving a practical convergence in 400 ms but without any overshoot. The convergence time is adaptively increased to ensure stability and 0% overshoot. These improvements highlight, specifically, no overshoot at the expense of a little higher convergent time, establishing the efficacy of the proposed adaptive ADRC framework.

Resilient control is indispensable for power converters in modern energy systems. Conventional and modern methods provide partial solutions, but ADRC offers a balanced framework of robustness and simplicity. Embedding finite-time convergence into ADRC elevates its capability, enabling converters to withstand uncertainties and disturbances with unprecedented speed and accuracy. This paper develops and validates a Han-inspired finite-time convergent ADRC, demonstrating its potential as a scalable solution for resilient power conversion, specifically achieving the following goals:

- Critical review of current ADRC frameworks using mathematical and analytical expressions.
- Design of adaptive ESO based on the adaptive error scaling function, achieving faster convergence during the span of large errors.
- Design of a finite-time convergent SMC-based control law using a smoother and customizable switching function.
- Stability proofs of the proposed ESO and the control law using Lyapunov stability theory and its variants, like singular perturbation theory and input-to-state stability theory.

- Applications of the proposed adaptive ADRC framework for moderately to highly nonlinear power converters.

The rest of the article is laid out as a standard research article. The next section, Section 2, presents the latest literature on current ADRC frameworks. Section 3 discusses in-depth theoretical aspects for the design and implementation of the proposed control system. Section 4 details extensive amounts of experimental results, and Section 5 completes the article by describing important conclusions and future recommendations.

## 2. Current State-of-the-Art in the Literature

The history of ADRC starts in the 1990s, but its extensive acceptance and theoretical evolution in the global research community was incited by a single, pivotal publication by Professor Han. This paper marks the *de facto* start of the modern ADRC era. The paper's primary contribution was not the invention of new mathematics, since the core ADRC concepts have existed for over a decade, but rather a strategic and philosophical *re-contextualization* of the framework. Han's central thesis was that ADRC is the natural, evolutionary successor to the PID controller [5].

This section provides a comprehensive overview of applications of ADRC in power converters. Firstly, it will present glimpses of ADRC developments from the literature, beginning with the era of Professor Han to the present. Secondly, the major problems involving converters will be presented within the context of control theory, and lastly, the role ADRC has played in mitigating them will be presented.

A general $n$-th order physical nonlinear system [6] can be described as follows:

$$y^{(n)} = f(t, y, \dot{y}, \ddot{y}, \dddot{y}, \ldots, y^{(n-1)}, u) \tag{1}$$

The system described in (1) is a general form for a non-autonomous system. According to sliding-mode control theory, any non-autonomous system could be facing matched uncertainty or unmatched uncertainty. In the case of the former condition, $f(t, y, \dot{y}, \ddot{y}, \dddot{y}, \ldots, y^{(n-1)}, u) = bu + d(t) = bu + d_m(t)$, and in the case of unmatched uncertainty, $f(t, y, \dot{y}, \ddot{y}, \dddot{y}, \ldots, y^{(n-1)}, u) = bu + d(t) = bu + [d_m(t) + g(y, t)]$, the system in (1) that is influenced by matched or unmatched uncertainties, $g(y, t)$, will get the following form:

$$y^{(n)} = bu + d(t) \tag{2}$$

The system in (2) can be transformed to ADRC framework by defining $x_1 = y$, $x_2 = \dot{y}$, $x_3 = \ddot{y}$, …, $x_n = y^{(n-1)}$. Then, we have the following:

$$\begin{aligned} \dot{x}_1 &= x_2 \\ \dot{x}_2 &= x_3 \\ &\vdots \\ \dot{x}_n &= x_{n+1} + bu \\ \dot{x}_{n+1} &= \dot{d}(t) \end{aligned} \tag{3}$$

In the expression above, the parameter $b$ is usually an estimated value, and the state $x_{n+1}$ represents the extended state, which is an accumulated estimation of the total disturbance. For this representation, it is assumed that $d(t)$ is continuous and differentiable. The system in (3) can be expressed in matrix form as follows:

$$\underbrace{\begin{bmatrix} \dot{x}_1 \\ \dot{x}_2 \\ \vdots \\ \dot{x}_n \\ \dot{x}_{n+1} \end{bmatrix}}_{\dot{x}} = \underbrace{\begin{bmatrix} 0 & 1 & 0 & \dots & 0 \\ 0 & 0 & 1 & \dots & 0 \\ \vdots & \vdots & \vdots & \ddots & \vdots \\ 0 & 0 & 0 & \dots & 1 \\ 0 & 0 & 0 & \dots & 0 \end{bmatrix}}_{A} \underbrace{\begin{bmatrix} x_1 \\ x_2 \\ \vdots \\ x_n \\ x_{n+1} \end{bmatrix}}_{x} + \underbrace{\begin{bmatrix} 0 \\ 0 \\ \vdots \\ b \\ 0 \end{bmatrix}}_{B} u + \underbrace{\begin{bmatrix} 0 \\ 0 \\ \vdots \\ 0 \\ 1 \end{bmatrix}}_{B_d} \dot{d}(t) \tag{4}$$

$$y = \begin{bmatrix} 1 & 0 & 0 & 0 & 0 \end{bmatrix} \begin{bmatrix} x_1 & x_2 & \dots & x_n & x_{n+1} \end{bmatrix}^T$$

The representation in (4) can easily be extended to incorporate MIMO systems.

### *2.1. Stability Determination Methods*

This section presents widely accepted stability theories like Lyapunov stability, singular perturbation theory, and input-to-state stability theory. These methods will help gauge the proposed control structures.

#### 2.1.1. Lyapunov Stability Theory (LST)

LST has been established as the fundamental theory for the determination of the stability of any system, for both linear and nonlinear systems. Since the ADRC framework in its pioneering form was an experimental scheme, LST has provided a theoretical foundation for the ADC framework [7]. A candidate Lyapunov function for a system with matched uncertainty [8,9] can be described as follows:

$$V = \frac{1}{2}\sum_{i=1}^{n}(e_i^{(i-1)})^2 + \frac{1}{2\gamma}\tilde{d}^2 \tag{5}$$

Here, $e_i = x_{d,i} - x_i$ and $\tilde{d} = d - \hat{d}$, such that $x_{d,i}$ is the desired state, and $x_i$ is the response state and $\tilde{d}$ represents the error in the estimated disturbance $\hat{d}$ given $d(t)$ is the actual disturbance. Similarly, for a system with unmatched uncertainty, the required Lyapunov function [10] is defined in a similar fashion as (5) with additional constraints:

$$\dot{V} \leq -\delta\|e\|^2 + \|e\|.\|g(y,t)\| \tag{6}$$

where $\delta > 0$ is a real constant. This approach guarantees that errors will either converge to zero or remain within a bounded region.

Convergence of the extended state observer (ESO) is often verified through foundational LST. If $\tilde{x}$ is the error between the state vector $x$ and its estimation $\hat{x}$, the Lyapunov function for the ESO can be defined as follows:

$$V = \frac{1}{2}\tilde{x}P\tilde{x} \tag{7}$$

where $P$ is the positive definite matrix, which usually depends on the ESO gains.

#### 2.1.2. Singular Perturbation Theory (SPT)

SPT provides a mathematical approach for systems with modes that operate at significantly different time scales. In ADRC, SPT divides error dynamics into slow (feedback) and fast (ESO) subsystems, with the ESO designed to react much quicker than the plant and controller [11]. By design, the observer dynamics are at least ten times faster than closed-loop dynamics. If $x = \begin{bmatrix} x_s^T & x_f^T \end{bmatrix}^T$ while $x_f$ is the state vector representing the faster

modes and $x_s$ is the state vector symbolizing the slower modes, then the LPT framework can be described as follows:

$$\begin{aligned} \dot{x}_s &= f_1(x_s, x_f, u) \\ \epsilon \dot{x}_f &= f_2(x_s, x_f, u) \end{aligned} \tag{8}$$

where $\epsilon = 1/\omega_0$ and $\omega_0$ is the bandwidth of the faster subsystem.

#### 2.1.3. Input-to-State Stability (ISS)

Input-to-state stability (ISS) is a widely recognized stability notion for nonlinear control systems that are subject to external inputs. A system is considered ISS if, in the absence of external inputs, it is globally asymptotically stable, and its trajectories remain bounded as a function of the input's magnitude for sufficiently long times [12]. For the system described in (4), ISS can be defined using the observer error, $\tilde{x} = x - \hat{x}$:

$$\|\tilde{x}(t)\|^2 \leq \beta\left(\|\tilde{x}(0)\|, t\right) + \gamma\left(\sup_{0 \leq t \leq \tau} \|d(t)\|\right) \tag{9}$$

where $\beta(.)$ and $\gamma(.)$ are K class functions (the functions that are monotonically decreasing) [13]. It states that if the observer dynamics satisfy ISS, the closed-loop system will be asymptotically stable.

### *2.2. ADRC Components*

This section outlines the evolution of ADRC as it exists today. A block diagram representation of the ADRC framework, indicating all components of the system, is shown in Figure 1. Because most advancements have occurred within individual ADRC components, key developments from the literature are discussed first.

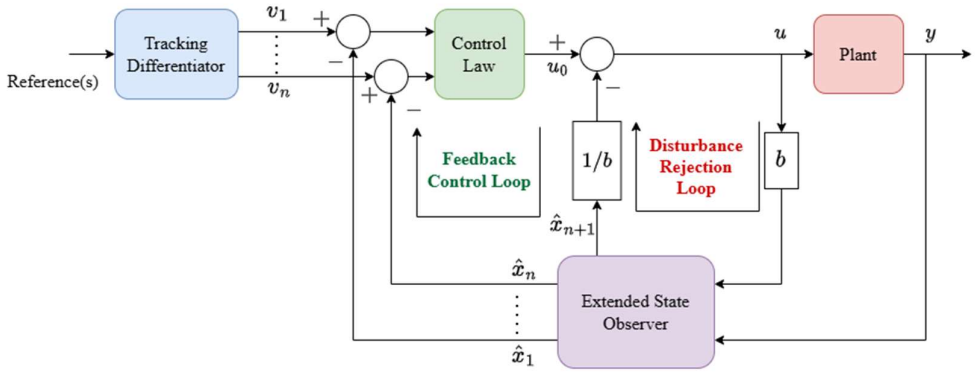



**Figure 1.** ADRC block diagram of major components of ADRC.

#### 2.2.1. Tracking Differentiator (TD)

TD, as shown in Figure 1, is a critical component of ADRC, primarily designed to generate a smooth transient profile for the reference signal that might contain sudden jumps [14].

Jingqing Han's original formulation of the TD, often referred to as Han-TD, is based on time-optimal control theory. For instance, for a double integral plant $\ddot{y} = u$, defined with state variables ($y = x_1$, $\dot{y} = x_2$) $\dot{x}_1 = x_2$, $\dot{x}_2 = u$, the time-optimal control input $u$ is given by the following(according to sliding-mode control (SMC) theory):

$$u = -r \operatorname{sign}\left(x_1 - v_0 + \frac{x_2|x_2|}{2r}\right) \tag{10}$$

where $v_0$ is the desired value for $x_1$, and $|u| \leq r$, whereas $r$ imposes the upper limit and limits the control signal $u$. According to Han, the sudden changes in the set-point can be

modeled using the double integrator dynamics, as described above [15]. Thus, the control law defined in (10) inspires the design of the TD formulation that can be used to generate the desired transient profile through the following differential equations:

$$\begin{aligned} \dot{v}_1 &= v_2 \\ \dot{v}_2 &= -r_1 \operatorname{sgn}\left(v_1 - v_0 + \frac{v_2|v_2|}{2r_1}\right) \end{aligned} \tag{11}$$

In this formulation, $v_1$ tracks the input signal $v_0(t)$, $v_2$ provides its approximate derivative, and the parameter $r_1$ controls the set-point change effects such that $|v_0| \leq r_1$. This unique structure was a key part of Han's early work [16].

The initial Han-TD presented practical challenges due to the discontinuity introduced by the sign() function, which can appreciate chattering. This issue spurred the evolution of TD, leading to several variants. The TD structure in (11) can be written in a generic form as follows:

$$\begin{aligned} \dot{v}_1 &= v_2 \\ \dot{v}_2 &= -a_{\text{des}}\, f(v_0,\, v_1,\, v_2) \end{aligned} \tag{12}$$

While the parameter $a_{\text{des}}$ and the function $f(v_0,\, v_1,\, v_2)$ are the design choices. An improved nonlinear tracking differentiator (INTD) was developed to circumvent the noise induced by the sign function, replacing it with a smoother hyperbolic tangent function [17,18]. The mathematical model for INTD is expressed as follows:

$$\begin{aligned} \dot{v}_1 &= v_2 \\ \dot{v}_2 &= -r_2^2 \tanh\left(\frac{\rho v_1 - (1-\epsilon)v_0}{\gamma}\right) - r_2 v_2 \end{aligned} \tag{13}$$

where $\rho$, $\epsilon$, $\gamma$, and $r_2$ are carefully chosen design parameters. It has been proven that the TD does make the control trajectory converge under the conditions: $r_2 > 0$, $\rho > 0$, $\gamma > 0$, $0 < \epsilon < 1$, and $|v_0| \leq r_2$.

To ensure faster and desired convergence, a TD formulation based on a sliding manifold $s(t) = cv_1 + v_2$ is presented by [19], which can be formulated as:

$$\begin{aligned} \dot{v}_1 &= v_2 \\ \dot{v}_2 &= -r_2 \tanh(a(v_1 - v_0)) - r_2 s(t) - c v_2 \end{aligned} \tag{14}$$

The parameters $r_2$, $a$, and $c$ are real and must be positive. Another research work proposes a TD structure defined as:

$$\begin{aligned} \dot{v}_1 &= v_2 \\ \dot{v}_2 &= -R^2\left[a_1(v_1 - v_0) - \tfrac{b_1}{R} v_2 - \tfrac{b_2}{R^n} v_2^n\right] \end{aligned} \tag{15}$$

While $a_1 > 0$, $b_1 > 0$, and $b_2 > 0$, and $n$ is an integer with $n > 0$. The convergence of the set-point profile is guaranteed with $|v_0| \leq R$. With different choices on $n$, several variants of (15) can be designed depending on the requirements of the control problem [20]. This idea presents huge flexibility without the inclusion of a nonlinear function, although it will be a nonlinear function for $n > 1$, [21,22].

An extensive amount of literature can be explored where linear versions of TD are proposed [23]. For instance, a TD formulation is defined as:

$$\begin{aligned} \dot{v}_1 &= v_2 \\ \dot{v}_2 &= -1.73\lambda v_2 - \lambda^3 (v_1 - v_0) \end{aligned} \tag{16}$$

Here, $\lambda$ is a parameter tuned to fit the specific transient profile requirements. It should be noted that the structure presented in (16) can be manipulated to become the one as proposed in (15). The forms presented in (15) and (16) have led to a generic structure of a linear TD framework:

$$\begin{aligned} \dot{v}_1 &= v_2 \\ \dot{v}_2 &= -\alpha_1(v_1 - v_0) - \alpha_2 v_2 \end{aligned} \tag{17}$$

The parameters $\alpha_1$ and $\alpha_2$ are the design parameters, which can be chosen to tune the bandwidth of the reference profile [24,25].

2.2.2. Extended State Observer (ESO)

ESO is the heart of the ADRC framework and its most significant innovation. ESO is a specialized state observer designed to estimate not only the conventional states of the system but also the augmented state representing the "total disturbance," using only the plant's input and output signals. Since it directly affects the robustness property of ADRC, it has inspired a higher amount of research as compared to other components of ADRC [26]. According to Han, if the equivalent degrees of the system in (4) is $n = 2$, its state estimator can be formulated as follows:

$$\begin{aligned} e &= \hat{x}_1 - y \\ \dot{\hat{x}}_1 &= \hat{x}_2 - \beta_{01}\mathrm{fal}(e, \alpha, \delta) \\ \dot{\hat{x}}_2 &= \hat{x}_3 - \beta_{02}\mathrm{fal}(e, \alpha, \delta) + b_0 u \\ \dot{\hat{x}}_3 &= -\beta_{03}\mathrm{fal}(e, \alpha, \delta) \end{aligned} \tag{18}$$

In this structure, $\hat{x}_1$ and $\hat{x}_2$ estimate the system states $x_1$ and $x_2$ respectively, $\hat{x}_3$ estimates the total disturbance $f(.)$, and $\beta_{01}$, $\beta_{02}$, and $\beta_{03}$ are the observer gains. The ESO in (18) is clearly nonlinear, and it delivers superior performance, particularly for unpredictable forms of error. The unprecedented performance is mainly caused by the $fal$ function, a nonlinear saturation function. Its general piecewise definition is:

$$\mathrm{fal}(e,\ \alpha,\ \delta) = \begin{cases} |e|^{\alpha}\mathrm{sign}(e) & , \quad |e| > \delta \\ \frac{e}{\delta^{1-\alpha}} & , \quad |e| \le \delta \end{cases} \tag{19}$$

In (18) and (19), $0 < \alpha < 1$ and $\delta > 0$. Some variations utilize polynomial functions for the region, $|e| \le \delta$ to ensure differentiability and continuity, addressing the non-smoothness at breakpoints that can affect control performance [27].

Subsequent refinements are aimed at mitigating practical issues like chattering while preserving the core advantages of ESO. In this context, a linear ESO (LESO) is inspired by the Leuenberger observer structure [28]. For a second-order system, the dynamics of LESO are given by:

$$\begin{bmatrix} \dot{\hat{x}}_1 \\ \dot{\hat{x}}_2 \\ \dot{\hat{x}}_3 \end{bmatrix} = \begin{bmatrix} 0 & 1 & 0 \\ 0 & 0 & 1 \\ 0 & 0 & 0 \end{bmatrix} \begin{bmatrix} \hat{x}_1 \\ \hat{x}_2 \\ \hat{x}_3 \end{bmatrix} + \begin{bmatrix} 0 \\ b_0 \\ 0 \end{bmatrix} u + \begin{bmatrix} l_1 \\ l_2 \\ l_3 \end{bmatrix} (y - \hat{x}_1) \tag{20}$$

The parameters $l_1$, $l_2$, and $l_3$ are the observer gains. LESO is favored for its simplified parameter-tuning compared to its nonlinear counterparts, making it more accessible in practical applications [29]. For ESO's bandwidth characterization, all poles of the ESO can be placed at one location. To make the ESO's transients considerably faster than closed-loop transients, $s^{ESO} \approx (3 \ldots 10)s^{CL}$, and therefore, $l_1 = -3s^{ESO}$, $l_2 = -3\left(s^{ESO}\right)^2$, and $l_3 = -\left(s^{ESO}\right)^3$. And the selection of $s^{CL}$, the closed-loop poles, could be dictated by the known plant limitations and speed and accuracy requirements [30].

The research work by [31] presents another variant of ESO, named the extended high-gain observer (EHGO). It is designed to operate at a faster rate than the extended system dynamics, which means they do not require disturbances to be slowly varying. An EHGO can be defined [32] as:

$$\begin{gathered}\dot{\hat{x}}_i = \hat{x}_{i+1} + \left(\frac{\alpha_i}{\epsilon_i}\right)(y - \hat{x}_1), \qquad 1 \le i \le n-1 \\ \dot{\hat{x}}_{i+1} = \phi_A(\boldsymbol{\eta}, \boldsymbol{x}, w) + \phi_B(\boldsymbol{\eta}, \boldsymbol{x}, w)u \\ y = x_1\end{gathered} \tag{21}$$

The values of the gain parameters $(\alpha_i/\epsilon_i)$ can be made larger by taking $1 < \alpha_i < \infty$ and $0 < \epsilon_i < 1$. The variables $x_i$ are the individual states, $\phi_A(\boldsymbol{\eta}, \boldsymbol{x}, w)$ is state transformation function, $\phi_B(\boldsymbol{\eta}, \boldsymbol{x}, w)$ is the control input $u$ transformation function, and $y$ is the output from the system. It is assumed that these functions are continuous and differentiable [33].

*Adaptive ESO (AESO)* is another variant to mitigate the issues of chattering and other things. AESO automatically adjusts its observer bandwidth based on the real-time voltage error, thereby balancing tracking performance and disturbance suppression. It increases bandwidth during periods of high error for faster convergence and decreases it during steady state (low error) for improved disturbance suppression [34]. For the system defined in (4), the dynamics of an adaptive ESO can be defined as:

$$\dot{\hat{\boldsymbol{x}}}(t) = A\hat{\boldsymbol{x}} + Bu + L(t)(y - \hat{y}) \tag{22}$$

whereas $L(t) = \begin{bmatrix}\beta_1(t) & \beta_2(t) & \dots & \beta_n(t) & \beta_{n+1}(t)\end{bmatrix}^{\mathrm{T}}$, $\beta_i(t) = \alpha_i \omega_0^i(t)$, and

$$\omega_0(t) = \omega_{MIN} + (\omega_{MAX} - \omega_{MIN})\sigma\left(\overline{\phi}(t)\right) \tag{23}$$

The parameters $\omega_{MIN}$ and $\omega_{MAX}$ define the bandwidth of the desired system, and the signal $\overline{\phi}(t)$ is defined to make $\omega_0(t)$ change adaptively [35]. One way of defining this signal is $\overline{\phi}(t) = \gamma_d|e(t)|$, where $\gamma_d$ is the design parameter [36]. The ultimate adaptivity is characterized by $\sigma(.)$, which can be defined as:

$$\begin{gathered}\sigma\left(\overline{\phi}(t)\right) = \frac{\overline{\phi}(t)}{1+\left|\overline{\phi}(t)\right|} \quad \text{or} \\ \sigma\left(\overline{\phi}(t)\right) = \operatorname{atan}\left(\overline{\phi}(t)\right) \quad \text{or} \\ \sigma\left(\overline{\phi}(t)\right) = \tfrac{1}{2}\left[1 + \tanh\left(\overline{\phi}(t)\right)\right]\end{gathered} \tag{24}$$

*Finite-Time ESOs (FTESOs)*, proposed by various researchers, are another class of observers that ensure the occurrence of convergence within a predictable time bound. However, the convergence time in FTESOs can be dependent on the initial conditions of the system. To ensure finite-time convergence, it can be defined as:

$$\begin{gathered}\dot{\hat{\boldsymbol{x}}} = f(\hat{\boldsymbol{x}}, u) + \hat{d} + L_1|e(t)|^{\alpha}\operatorname{sign}(e(t)) \quad \text{and} \\ \dot{\hat{d}} = L_2|e(t)|^{\beta}\operatorname{sign}(e(t))\end{gathered} \tag{25}$$

where $L_1$ and $L_2$ are observer gains and $\alpha,\ \beta \in (0, 1)$ [37,38].

FTESO has also inspired the formulation of fixed-time ESO (FXTESO). Building upon FTESO, FXTESO guarantees convergence within a predefined fixed time, irrespective of the initial conditions [39]. For a system defined in (4), an FXTESO can be defined as:

$$\begin{gathered}\dot{\hat{\boldsymbol{x}}} = f(\hat{\boldsymbol{x}}, u) + \hat{d} + L_1|e(t)|^{\alpha}\operatorname{sign}(e(t)) + L_2|e(t)|^{\beta}\operatorname{sign}(e(t)) \quad \text{and} \\ \dot{\hat{d}}' = L_3|e(t)|^{\gamma}\operatorname{sign}(e(t)) + L_3|e(t)|^{\eta}\operatorname{sign}(e(t))\end{gathered} \tag{26}$$

where $L_i$, $i = 1,2,3,4$ are observer gains and $\alpha$, $\beta$, $\gamma$, $\eta \in (0,1)$. The convergence is completely controllable by the designer and does not depend on the initial conditions [40].

Another ESO is the *Disturbance-Compression ESO (DC-ESO)*, which directly modifies the characteristics of disturbance encountered by the observer, thus reducing the upper bounds of the disturbance and its derivative. This innovation directly addresses the conflict between high-gain observation and noise sensitivity, allowing for comparable estimation errors with substantially lower observer gains than conventional ESOs [41].

The standard $n$-th order LADRC uses an $(n+1)$-th order LESO. This is computationally necessary when only the output $y$ is measured. However, in many applications, several states are directly measurable [42]. The Reduced-Order ESO (RESO) provides a method to reduce the observer's order and computational cost by leveraging these additional measurements. If $k$ states are measurable, the ESO order can be reduced from $(n+1)$ to $(n+1-k)$. This RESO is computationally cheaper and can be faster. However, the inherent noise in the output signal can get into the controller, thus affecting the performance of the controller, whereas the full-order LESO's internal structure has a filtering effect. But RESO is ideal for embedded systems where CPU cycles are a concern, but the sensor noise must be low [43].

A more recent and "research-frontier" development is the introduction of fractional calculus into the ADRC framework. This replaces the integer-order integrators in the controller or observer with fractional-order operators ($1/s^{\alpha}$ where $\alpha \in \mathbb{R}$). Fractional-Order ADRC (FO-ADRC) provides additional degrees of freedom, which can be used to fine-tune the controller's robustness and performance. A standard LADRC has two *knobs* ($\omega_o$, and $\omega_c$). A FO-LADRC can have five or more such parameters to be tuned [44].

FO-ADRC allows a much "flatter" phase response around the crossover frequency, which is known to improve robustness to gain variations [45]. While theoretically promising, FO-ADRC is more computationally intensive to implement (requiring approximations like Oustaloup's filter), and its tuning is significantly more complex, moving it away from the simplicity that made LADRC popular [46].

ESOs have demonstrated high effectiveness in estimating system states and uncertainties, which directly translates into improved tracking performance through a mechanism of direct compensation.

#### 2.2.3. Feedback Control Law

ADRC extends the traditional PID framework by incorporating a nonlinear state error feedback mechanism. Indeed, early seminal works often referred to ADRC as a form of nonlinear PID control. The fundamental design principle of the ADRC law involves two primary steps: first, actively canceling the estimated total disturbance, and then applying a stabilizing controller to the resulting simplified plant, which effectively becomes a chain of integrators [47].

A general active disturbance rejection law can be formulated as:

$$u = \frac{(u_0 - \hat{x}_{n+1})}{b_0} \tag{27}$$

In Equation (35), $\hat{x}_{n+1}$ is the extended state that estimates the system's disturbances and $u_0$ is the control signal, which could be a linear or nonlinear function of the error signal. One way of implementing this control signal is [48]:

$$u_0 = K_P fal(e) - K_D fal(e) \tag{28}$$

ADRC's initial designs favored nonlinear gain structures, recognizing their potential to better accommodate dynamic uncertainties and disturbances. The $fal\ (.)$ function, a key

nonlinear element, was designed to provide a "small error, large gain; large error, small gain" characteristic [49]. This property aims to enhance performance and robustness, even for linear plants, by applying higher control effort for small errors to drive them quickly to zero, while limiting gain for large errors to prevent saturation or instability [50].

However, the non-smooth nature of the original $fal(.)$ function at its breakpoints could introduce practical issues such as chattering, which might degrade control performance. This led to continuous efforts to refine the nonlinear feedback mechanisms [51]. Improvements included the adoption of smoother functions, such as hyperbolic tangent functions [52] (as seen in some TD variants) or piecewise polynomial functions [53] for the $fal(.)$ function itself. These modifications aimed to mitigate chattering while retaining the performance benefits of nonlinearity. This ongoing refinement demonstrates the imperative of engineering to make theoretical advantages practically viable, continuously optimizing the trade-off between the performance gains from nonlinearity and the challenges of real-world implementation [54].

Some specific developments directed to the overall ADRC framework have also been noted. This paragraph represents the developments which indicate the usability of the adaptive ADRC in one way or the other. For instance [55], proposes a control law based on linear ESO to bring adaptivity and robustness. The research works by [56,57] present the design of ESO which brings direct adaptiveness in the control. The work by [28] proposes the inclusion of output filtering action before the implementation of the ESO. The research published by [58] adopts reinforcement learning in ESO and the control to inculcate adaptiveness. A summary of important research works is presented in Table 1.

**Table 1.** Summary of related research works.

| Ref. | Year | TD | ESO | Control Law | Remarks |
|---|---|---|---|---|---|
| [27] | 2009 | Nonlinear based on the sign function as defined in (11). | The observer based on $fal$-function defined in (19). | Control law based on $fhan$-function, and some other nonlinear variants. | This is the base work that triggered the research with the notion of active disturbance rejection control. |
| [29] | 2023 | Not implemented. | Linear ESO. | Data-driven control using dynamic disturbances identification. | Most implementations of the control framework are based on linear or linearized models. |
| [30] | 2013 | Not implemented. | Leuenberger-based linear ESO. | Linear PD-inspired control law. | This work inspired the linear implementation of the ADRC framework. |
| [31] | 2025 | Not implemented. | Exponential extended high-gain observer design. | Linear control based on efficiently estimated system states. | Good work, particularly contributing to the novelty in ESO. |
| [34] | 2022 | Not implemented. | Adaptive ESO is implemented as defined in Equations (23)–(26). | Linear control law is implemented. | The parameters of ESO are changed using the inverse-tangent function or tan-hyperbolic function. |
| [38] | 2024 | Not implemented. | Adaptive and finite-time ESO as defined in (27). The adaptiveness and finite-time converging properties are implemented using the product of a sign function and a nonlinear error function. | Sliding-mode-inspired control law based on nonlinear sliding manifolds and sign-switching function. | Great work implementing finite-time convergence and adaptivity using a non-smooth switching function. |
| [40] | 2023 | Fixed-time differentiator. | Implementation of AESO, as implemented in [38], but with more aggressive nonlinear action based on the sign function. | SMC-inspired linear control law based on sign function. | Good work but implemented using aggressive and nonlinear actions. |
| [55] | 2022 | Not implemented. | Linear ESO. | SMC-inspired control law using smooth sign function. | The control framework worked well for the problem at hand, as outlined in the article. |
| [56] | 2023 | Not implemented. | Adaptive ESO whose parameters are adjusted by a deep reinforcement learning agent using deep deterministic policy gradient. | Linear control law where control parameters are adjusted by a deep reinforcement learning agent using deep deterministic policy gradient. | Great work, but computationally complex and demanding higher computational resources and energy. |

**Table 1.** *Cont.*

| Ref. | Year | TD | ESO | Control Law | Remarks |
|---|---|---|---|---|---|
| [57] | 2022 | Not implemented. | Adaptive ESO based on a nonlinear sign-function. | Adaptive control using linear sliding surfaces and a sign-function reaching law. | Adaptiveness is embedded in ESO and the control law using a hard-switching sign-function. |
| [28] | 2023 | Not implemented. | Linear ESO, but the extended state is estimated with an additional 1st-order filtering action. | Linear control law. | The inclusion of the filter helps reduce huge spikes in the estimation of the extended state, but at the cost of an additional pole in the system. |
| [58] | 2023 | Han-TD as proposed in [27]. | Han-ESO as proposed in [27]. | Han-nonlinear control law as proposed in [27]. | The researcher has set a deep reinforcement learning network to update the parameters of ADRC components. |

After a detailed review of different developments and their application in the literature, it can be concluded that ADRC is inspiring great control strategies for a diverse range of control problems. ESO remained the target of more developments than the control or the tracking differentiator. Some works have also been inspired by the sliding-mode control theory for the design of finite-time convergent ESO and control laws. Most researchers have proposed the design of ESO, control law, or both using a hard-switching sign-function. There are a few researchers who have contributed to the development of adaptive ESO and adaptive control laws using smooth switching functions like the inverse tangent function or tangent-hyperbolic function. This work is motivated by the deployment of smooth functions that are designed using a sigmoidal function for the realization of adaptive ESO and the adaptive control law. Specifically, the proposed ADRC system will demonstrate that all states of the system can be controlled without affecting the response from the other states.

## 3. Methodology—Control System Design

In this section, the focus is on the detailed design and implementation process of the proposed ARDC control scheme. The section begins by formally introducing the control framework, ensuring that each component and its role within the overall system are clearly defined. After the control law is presented, rigorous proofs regarding the stability and effectiveness of both the control law and the extended state are provided. These proofs are essential to demonstrate the theoretical soundness of the proposed approach. Additionally, the methodologies employed in designing both the control law and the extended state are explained step by step. This includes outlining the rationale behind the chosen design strategies and highlighting how each method contributes to the overall performance and robustness of the ARDC control scheme.

### *3.1. Proposed Adaptive ADRC Framework and Its Stability Analysis*

Before the proposed control structure is presented, it will be worthwhile defining the novel switching and error scaling function.

**Definition 1.** *A smooth, continuous, and differentiable switching function $\phi(x)$ can be defined as:*

$$\phi(x) = a_\phi + \frac{b_\phi}{1 + \exp(-\mu x)}$$

*The function has the following properties:*

- $a_\phi > b_\phi; b_\phi < 0.$
- $\lim_{x \to -\infty} \phi(x) = a_\phi = h_U.$
- $\lim_{x \to 0} \phi(x) = a_\phi + \frac{1}{2} b_\phi.$

- $\lim_{x \to +\infty} \phi(x) = a_\phi + b_\phi = h_L$.

The parameter $\mu$ can be selected to set the speed of switching. A plot of the switching function for $a_\phi = 1$, $b_\phi = -2$, and for different values of $\mu$ is shown in Figure 2. It should be noted that conventionally $|h_L| = |h_U|$; however, the parameters $a_\phi$ and $b_\phi$ can be selected to not only break this convention, but also to be used to set the gain of the switching action.

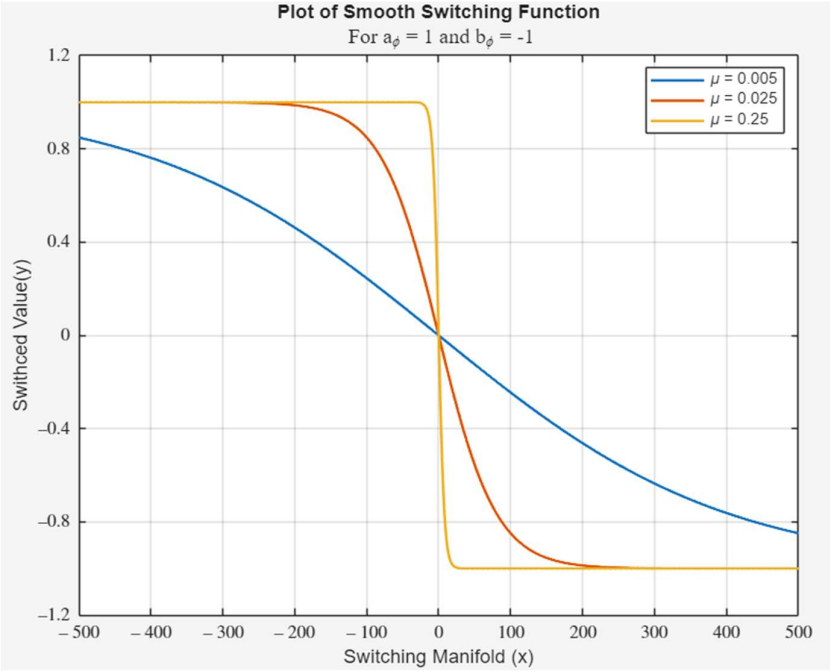



**Figure 2.** Plot of switching function.

**Definition 2.** *A continuous, differentiable, and monotonically increasing error scaling function $\varphi(x)$ can be defined, for the design of adaptive ESO, as:*

$$\varphi(x) = a_\varphi + \frac{2b_\varphi}{1+\exp(-\mu|x|)}$$
$$\lim_{\tilde{x}_1 \to \pm\infty} \varphi(x) = a_\varphi + 2b_\varphi = g_U$$
$$\lim_{\tilde{x}_1 \to 0} \varphi(x) = a_\varphi + b_\varphi = g_L$$

*It should be noticed that the parameters $a_\varphi$ and $b_\varphi$ are selected such that $0 < g_L < \varphi(x) \leq g_U$, $0 < g_L < 1$, and $1 < g_U \leq 2$. A plot of the function for $a_\varphi = -0.3$, and $b_\varphi = 1$. It is also pointed out that the error scaling function in Definition 2 is a variant of the smooth switching function described in Definition 1.*

#### 3.1.1. Proposed Adaptive ADRC Framework

The error dynamics of the ADRC dynamic system (with $n = 2$) defined in (4) can be described as:

$$\begin{aligned} \dot{e}_1 &= e_2 \\ \dot{e}_2 &= \dot{x}_{d2} - x_3 - bu \end{aligned} \tag{29}$$

whereas $e_1 = x_{d1} - x_1$, $e_2 = \dot{e}_1 = \dot{x}_{d1} - \dot{x}_1 = x_{d2} - x_2$, $\dot{x}_{d2}$ is the derivative of second reference signal, $x_3$ represents the extended state, and $u$ is the control signal and $b$ is the

coefficient of the control signal. A sliding surface $\sigma(t)$ and a reaching law $\dot{\sigma}(t)$ based on the error dynamics in (29) are defined as:

$$\begin{aligned} \text{Sliding Surface :} \quad & \sigma(t) = c_1 e_1 + e_2 \\ \text{Reaching Law :} \quad & \dot{\sigma}(t) = -k_1 \sigma - \epsilon \phi(\sigma(t)) \end{aligned} \tag{30}$$

where $c_1 > 0$ is the coefficient $e_1$, $k_1 > 0$ is the coefficient of the sliding surface, and $\epsilon > 0$ is the coefficient of the switching function that controls the chattering and reaching speed. Taking derivative $\dot{\sigma}(t)$ and equating the two components of (30), the proposed nonlinear control law is obtained:

$$\begin{aligned} u &= \tfrac{1}{b}\left[c_1 e_2 + \dot{x}_{d2} - x_3 + k_1 \sigma(t) + \epsilon \phi(\sigma(t))\right] \\ &= \tfrac{1}{b}\left[\dot{x}_{d2} + k_1 c_1 e_1 + (k_1 + c_1) e_2 - x_3 + \epsilon \phi(\sigma(t))\right] \end{aligned} \tag{31}$$

If $\hat{x}_i; i = 1, 2, 3$ are the estimations of the states $x_i; i = 1, 2, 3$, then, inspired by Professor Han, an ESO can be defined as:

$$\begin{aligned} \dot{\hat{x}}_1 &= \hat{x}_2 + \beta_1(\widetilde{x}_1)\varphi(\widetilde{x}_1) \\ \dot{\hat{x}}_2 &= \hat{x}_3 + \beta_2(\widetilde{x}_1)\varphi(\widetilde{x}_1) + bu \\ \dot{\hat{x}}_3 &= \beta_1(\widetilde{x}_1)\varphi(\widetilde{x}_1) \end{aligned} \tag{32}$$

where $\widetilde{x}_1 = y - \hat{x}_1 = x_1 - \hat{x}_1$ and the parameters $\beta_i$ are selected such that $s^3 + \beta_1 s^2 + \beta_2 s + \beta_3 = 0$ forms the characteristic equation of the linear ESO defined in (32). The states $\hat{x}_2$ and $\hat{x}_3$ are the estimates of $x_2$ and $x_3$ respectively. The function $\varphi(\widetilde{x}_1)$ works as the adaptive scaling function. If the error is larger, it helps with faster convergence, as is evident from Definition 2 and Figure 3. A block diagram representation of the proposed control framework is shown in Figure 4.

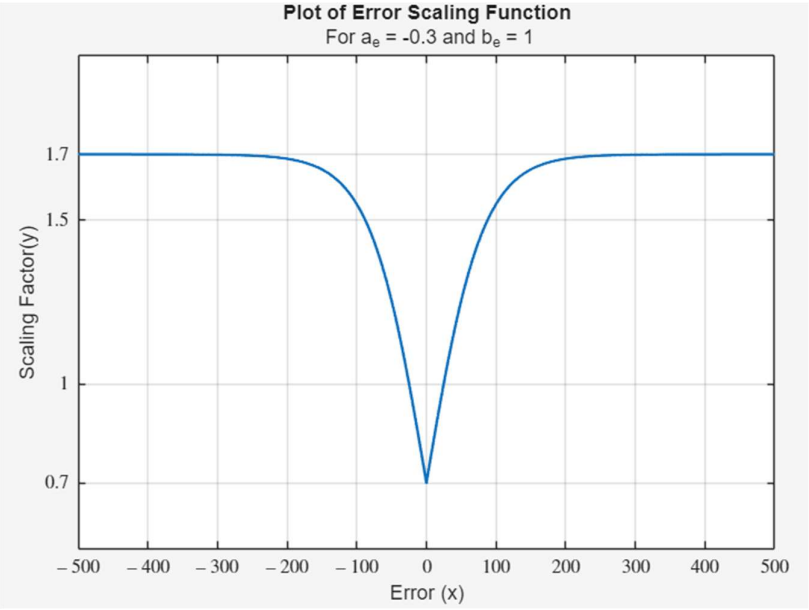



**Figure 3.** Error scaling function.

The stability proofs in the next subsection will demonstrate that the proposed controller, and the ESO will be able to converge to the origin. Therefore, it is also possible that the proposed ADRC framework will make plausible the tracking of both output voltage

and current reference signals. This latter point will be demonstrated using simulation experiments in Section 4.

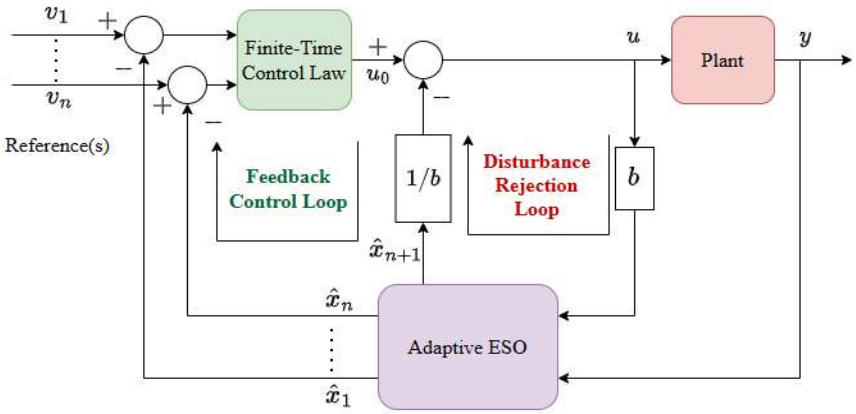



**Figure 4.** Proposed ADRC scheme.

3.1.2. Stability Analysis of Control Law

Stability proofs in nonlinear control theory rely on the Lyapunov energy function, enabling researchers to show that its derivative is consistently negative, confirming stability. However, it can be challenging to find negative values for the Lyapunov function, particularly for cases where a custom-designed switching function is used, as in this work. The definitions below offer guidance for developing stability proofs in such cases.

After the formal description of the proposed active disturbance rejection control system, the stability proofs of the control law and the observer dynamics are presented. The stability proof of the control law is presented using two definitions of the Lyapunov function and by also using the input-to-state stability theory.

From Equations (29) and (31), the closed-loop error dynamics will become:

$$\begin{aligned} \dot{e}_1 &= e_2 \\ \dot{e}_2 &= -c_1 e_2 - k_1 \sigma(t) - \epsilon \phi(\sigma(t)) \end{aligned} \tag{33}$$

The closed-loop error equations in (41) indicate the stabilizing and converging dynamics, but their stability will be verified using Lyapunov stability theory.

**Definition 3.** *For any real values, $p$ and $q$ with some positive constants $\xi$ and $n_1$, Young's inequality* [59] *is defined as:*

$$pq \leq \xi p^2 + \frac{1}{n_1 \xi} q^2;\ 0 < \xi < 1,\ n_1 > 4$$

**Definition 4.** *For a real nonlinear function $f(p)$, a sector condition* [60,61] *is defined as:*

$$\begin{aligned} (\mathrm{A}):\ & m_1 f^2(p) \leq p f(p) \leq m_2 f^2(p);\ 0 < m_1 < m_2 \\ (\mathrm{B}):\ & m_1 f^2(g(p)) \leq p f(g(p)) \leq m_2 f^2(g(p));\ 0 < m_1 < m_2 \end{aligned}$$

The stability of the control law in (39) can be evaluated using a Lyapunov function $V_c = \frac{1}{2}\left[e_1^2 + e_2^2\right]$, and then using closed-loop error dynamics in (33), it can be shown that:

$$\dot{V}_c = (1 - k_1 c_1) e_1 e_2 - (k_1 + c_1) e_2^2 - \epsilon e_2 \phi(\sigma)$$

Using Young's inequality from Definition 3 and sector condition from Definition 4, the above expression can be written as (also noting that $k_1c_1 \gg 1$):

$$\dot{V}_c \leq -k_1c_1\left(\xi e_1^2 + \frac{1}{n_1\xi}e_2^2\right) - (k_1 + c_1)e_2^2 - \epsilon\xi e^2 - \frac{\epsilon}{n_1\xi}\phi^2(\sigma(e))$$

Collecting like terms:

$$\dot{V}_c(\boldsymbol{e}) \leq -\xi k_1c_1e_1^2 - \left[\frac{k_1c_1}{n_1\xi} + (k_1 + c_1) + \epsilon\xi\right]e_2^2 - \frac{\epsilon}{n_1\xi}\phi^2(\sigma(e)) \tag{34}$$

The derivative of the Lyapunov function is negative for all error conditions, and thus, the control law stabilizes the closed-loop system asymptotically. Next, an expression for the convergence time is developed. For the development of an expression for the time of convergence, the following assumptions are made.

**Assumption 1.** *Since* $0 < \xi < 1$, *error dynamics and, in turn,* $V_c(\boldsymbol{e})$, *the energy dynamics in (42) can be approximated as:*

$$\dot{V}_c \leq -2\xi k_1c_1\left[\frac{1}{2}\left(e_1^2 + e_2^2\right)\right] - \frac{\epsilon}{n_1\xi}\phi^2(\sigma)$$

**Assumption 2.** *With reference to Definition 1 and Figure 2, we have the following:*

$$\lim_{t\to\infty}\boldsymbol{e}(t) = 0 \implies \sigma(t) \to 0 \implies \phi(\sigma) \to 0$$

In accordance with the above two assumptions, we have the following:

$$\dot{V}_c \leq -2\xi k_1c_1V_c$$

Solving the above equation, we get the following:

$$V_c(t) \leq V_c(0)\exp(-2\xi k_1c_1t) \quad \implies \quad T_{cvg} \approx \frac{2}{\xi k_1c_1} \tag{35}$$

The above analysis clearly demonstrates that the proposed control law is globally asymptotically stabilizing with a finite-time convergence, and it is independent of initial conditions. The structure of the switching function described in Definition 1 also plays a definitive role in this convergence.

The convergence of the control law can also be proved by defining the Lyapunov function using the definition of the sliding manifold from Equation (29):

$$V_\sigma = \frac{1}{2}\sigma^2 \implies \dot{V}_\sigma = \sigma\dot{\sigma}$$

Now, we use open-loop error dynamics from (33) and control law from (31), with the fact that it is based on estimated states (i.e., perfect cancellation of total disturbance represented by $x_3$ does not occur, and the cancellation error is $\tilde{x}_3 = x_3 - \hat{x}_3$):

$$\dot{V}_\sigma = -k_1\sigma^2 - \epsilon\sigma\phi(\sigma) - \sigma\tilde{x}_3$$

Using Definition 3 and Definition 4 on the last two terms, we have the following:

$$\dot{V}_\sigma \leq -k_1\sigma^2 - \epsilon m_1\phi^2(\sigma) - \xi\sigma^2 - \frac{1}{n_1\xi}\tilde{x}_3^2 = -(k_1 + \xi)\sigma^2 - \frac{1}{n_1\xi}\tilde{x}_3^2 - \epsilon m_1\phi^2(\sigma) \tag{36}$$

From Equation (36), the stability analysis clearly indicates that the control law is also stabilizing with this definition of the Lyapunov function. But $\tilde{x}_3$ is a disturbance input, and it will have a certain impact on the states' stability under the framework of input-to-state stability (ISS). The term $\epsilon m_1 \phi^2(\sigma)$, according to Assumption 2, will converge to zero, and so its impact can be ignored. Therefore, Equation (36) can be rewritten using the definition of the Lyapunov function $V_\sigma = 1/2\sigma^2$ as:

$$\dot{V}_\sigma \leq -2(k_1 + \xi)V_\sigma - \frac{1}{n_1 \xi}\tilde{x}_3^2 \tag{37}$$

Since $0 < \xi < 1$, $n_1 > 4$ (according to Definition 3), and $k_1 > 0$, the second term will assume large values. Therefore, the control law will be globally stabilizing, even under the presence of $\tilde{x}_3$.

3.1.3. Stability Analysis of Adaptive ESO

In this section, the stability analysis of proposed ESO is described using LST and SPT. Before the stability analysis for ESO is presented, some definitions are required.

**Definition 5.** *Using the definitions in (4) for $n = 2$, estimated state dynamics from (40), and estimated state errors: $\tilde{x}_1 = x_1 - \hat{x}_1$, $\tilde{x}_2 = x_2 - \hat{x}_2$, $\tilde{x}_3 = x_3 - \hat{x}_3$, the estimation error dynamics can be described as:*

$$\begin{aligned}
\dot{\tilde{x}}_1 &= \tilde{x}_2 - \beta_1 \tilde{x}_1 \varphi(\tilde{x}_1) \\
\dot{\tilde{x}}_2 &= \tilde{x}_3 - \beta_2 \tilde{x}_1 \varphi(\tilde{x}_1) \\
\dot{\tilde{x}}_3 &= w(t) - \beta_3 \tilde{x}_1 \varphi(\tilde{x}_1)
\end{aligned}$$

*where $\dot{x}_3 = \dot{f}(t) = w(t)$.*

**Definition 6.** *The high-gain parameters $\beta_i$, $i = 1, 2, 3$ can be written as $\beta_1 = \frac{\alpha_1}{\varepsilon}$, $\beta_2 = \frac{\alpha_2}{\varepsilon^2}$, and $\beta_3 = \frac{\alpha_3}{\varepsilon^3}$, and then the estimation error dynamics will be:*

$$\begin{aligned}
\dot{\tilde{x}}_1 &= \tilde{x}_2 - \tfrac{\alpha_1}{\varepsilon} \tilde{x}_1 \varphi(\tilde{x}_1) \\
\dot{\tilde{x}}_2 &= \tilde{x}_3 - \tfrac{\alpha_2}{\varepsilon^2} \tilde{x}_1 \varphi(\tilde{x}_1) \\
\dot{\tilde{x}}_3 &= w(t) - \tfrac{\alpha_3}{\varepsilon^3} \tilde{x}_1 \varphi(\tilde{x}_1)
\end{aligned}$$

**Definition 7.** *The parameter ε can be used to bifurcate the slower and faster dynamics by defining the fast timescale as $\tau = t/\varepsilon \implies d/dt = d/\varepsilon d\tau$. Let the fast derivative be denoted as prime notation, then we have the following:*

$$\begin{aligned}
\tilde{x}_1' &= \varepsilon \dot{\tilde{x}}_1 = \varepsilon \tilde{x}_2 - \alpha_1 \tilde{x}_1 \varphi(\tilde{x}_1) \\
\tilde{x}_2' &= \varepsilon \dot{\tilde{x}}_2 = \varepsilon \tilde{x}_3 - \tfrac{\alpha_2}{\varepsilon} \tilde{x}_1 \varphi(\tilde{x}_1) \\
\tilde{x}_3' &= \varepsilon \dot{\tilde{x}}_3 = \varepsilon w(t) - \tfrac{\alpha_3}{\varepsilon^2} \tilde{x}_1 \varphi(\tilde{x}_1)
\end{aligned}$$

Using LST framework in (7), a Lyapunov function for ESO in [43], based on Definition 5, can be described as:

$$V_O = \frac{1}{2}[\tilde{x}_1^2 + \tilde{x}_2^2 + \tilde{x}_3^2] \tag{38}$$

Then, the derivative of this energy function in (38) with the help of Definition 6 will be:

$$\dot{V}_O = \widetilde{x}_1\widetilde{x}_2 - \frac{\alpha_1}{\varepsilon}\widetilde{x}_1^2\varphi(\widetilde{x}_1) + \widetilde{x}_2\widetilde{x}_3 - \frac{\alpha_2}{\varepsilon^2}\widetilde{x}_1\widetilde{x}_2\varphi(\widetilde{x}_1) + \widetilde{x}_3 w(t) - \frac{\alpha_3}{\varepsilon^3}\widetilde{x}_1\widetilde{x}_3\varphi(\widetilde{x}_1) \tag{39}$$

**Assumption 3.** *From Definition 2, it should be that the function $\varphi(\widetilde{x}_1)$ will always assume a positive value, and let that value be $\varphi(\widetilde{x}_1) = \overline{\varphi}$.*

Now, using Young's inequality from Definition 3 on product terms, use the sector condition from Definition 3 on $\widetilde{x}_3 w(t)$, Assumption 3, and collect like terms:

$$\dot{V}_O \leq -\left(\frac{\alpha_1\overline{\varphi}}{\varepsilon} + \frac{\alpha_2\overline{\varphi}\xi}{\varepsilon^2} + \frac{\alpha_3\xi}{\varepsilon^3} - \xi\right)\widetilde{x}_1^2 - \left(\frac{\alpha_2\overline{\varphi}}{n_1\xi\varepsilon^2} - \frac{1}{n_1\xi} - \xi\right)\widetilde{x}_2^2 - \left(\frac{\alpha_3\overline{\varphi}}{n_1\xi\varepsilon^3} - \frac{1}{n_1\xi} - \kappa\right)\widetilde{x}_3^2 \tag{40}$$

Clearly, as the transients progress, $\dot{V}_O \leq 0$. With appropriate manipulations, the above expression can approximately be written as:

$$\dot{V}_O \leq -\frac{\lambda_1}{\varepsilon_1}V_O$$

Therefore, an approximate value of the convergence time will be:

$$T_{cvg} \approx \frac{4\varepsilon_1}{\lambda_1} \tag{41}$$

Now the stability proof for the observer in (32) under singular perturbation theory (SPT) is presented. In the light of Definition 7, and assuming $\varepsilon \to 0$, the derivative of the Lyapunov function will be:

$$V_O' = -\frac{\alpha_1}{\varepsilon}\widetilde{x}_1^2\varphi(\widetilde{x}_1) - \frac{\alpha_2}{\varepsilon^2}\widetilde{x}_1\widetilde{x}_2\varphi(\widetilde{x}_1) - \frac{\alpha_3}{\varepsilon^3}\widetilde{x}_1\widetilde{x}_3\varphi(\widetilde{x}_1)$$

The time scale of the derivative $V_O'$ is different than $\dot{V}_O$. Again, we use Young's inequality from Definition 3 on product terms, using the sector condition in first terms from Definition 4, and using Assumption 3:

$$V_O' \leq -\left(\frac{\alpha_1\overline{\varphi}}{\varepsilon} + \frac{\alpha_2\overline{\varphi}\xi}{\varepsilon^2} + \frac{\alpha_3\xi}{\varepsilon^3}\right)\widetilde{x}_1^2 - \left(\frac{\alpha_2\overline{\varphi}}{n_1\xi\varepsilon^2}\right)\widetilde{x}_2^2 - \left(\frac{\alpha_3\overline{\varphi}}{n_1\xi\varepsilon^3}\right)\widetilde{x}_3^2$$

All terms are highly negative and, thus, stabilizing. This conclusion proves that fast dynamics are also stable.

### *3.2. Control System Design for Different Power Converters*

This section is dedicated to the design of the proposed ADRC framework for different power converters, such as buck converters, boost converters, and single-phase inverters. A block diagram of the controller indicating ESO and the control law is shown in Figure 5. The block diagram is based on the control law in (31) and ESO in (32).

#### 3.2.1. Adaptive ADRC Design and Implementation for Buck Converter

This converter circuit is designed to deliver a power of 7.6 kW at a switching frequency of 100 kHz. The input voltage to the converter is 380 V and the required output from the converter is 96 V. Design specifications and the resulting filtering (inductor and capacitor) and switching components (MOSFET and diode) are listed in Table 2. The switching devices have been selected to meet voltage, current, and frequency requirements under the worst-case conditions. The selected MOSFET can handle an average current of 127 A at 25 °C,

but this current must be derated down to 75%, and thus, the MOSFET can safely be loaded at 95.25 A (according to the datasheet, this limit is 89.3 A). Similarly, its drain-to-source must also be derated to 50% of its rated value of 1200 V. Thus, for the long life of the device, its drain-to-source voltage should not exceed 600 V. Thus, the selected device meets the requirements of all converters used in this work. The selected diode is rated at a forward current of 120 A and reverse breakdown voltage of 1200 V. Safety and long-life requirements dictate that its forward current should not exceed 90 A and its breakdown voltage should not exceed 600 V (these requirements have been set by different defense and aerospace organizations). Similarly, the current rating for the inductor and the voltage rating for the capacitor must not be exceeded to 50% of their rated values. The selected components meet these requirements. Other than these, both inductor and capacitor devices should be selected such that the energy storage capacities are never exceeded.

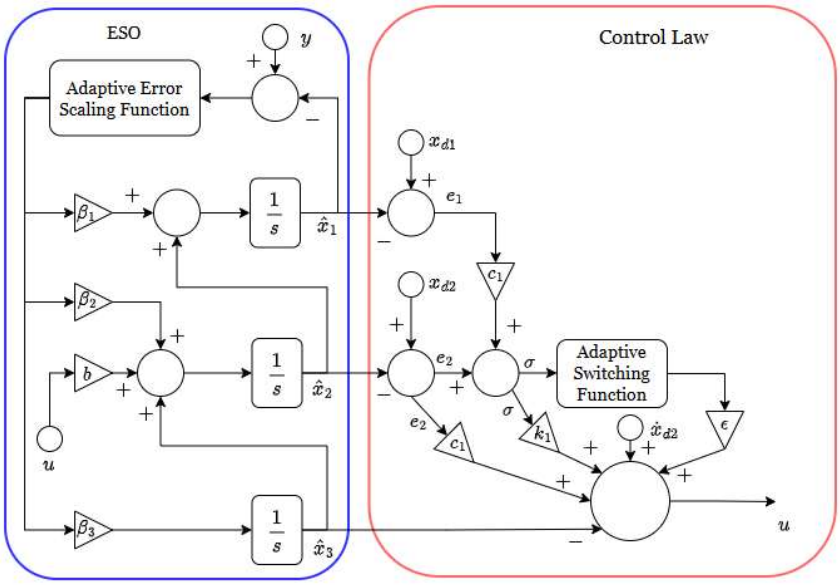



**Figure 5.** Controller scheme block diagram.

**Table 2.** Design specifications for buck and boost converters.

| Parameter | Value | Parameter | Value |
|---|---|---|---|
| Power Rating | 7.5 kW | Switching Frequency | 100 kHz |
| Inductor Current Ripple | <20% | Output Voltage Ripple | <0.5% |
| Diode | IDWD120E120D7 | MOSFET | IMW120R014M1H |
| **Buck Converter** | | **Boost Converter** | |
| Input Voltage | 380 V | Input Voltage | 96 V |
| Output Voltage | 96 V | Output Voltage | 380 V |
| Load Current | 80 A | Load Current | 20 A |
| Inductance | 68 µH | Inductance | 120 µH |
| Capacitance | 91 µF | Capacitance | 1800 µF |

If $V_O(s) = \mathcal{L}\{v_o(t)\}$ is the output voltage from a buck converter and $k_{dc}(s) = \mathcal{L}\{k_{dc}(t)\}$ is the duty cycle, the transfer function of the converter is described as [the operator $\mathcal{L}\{f(t)\}$ is the Laplace transform operator]:

$$G_{buck}(s) = \frac{V_O(s)}{k_{dc}(s)} = \frac{\frac{V_{in}}{LC}}{s^2 + \frac{1}{RC}s + \frac{1}{LC}} \implies \ddot{v}(t) = \underbrace{-\frac{1}{RC}\dot{v}(t) - \frac{1}{LC}v(t)}_{f(t)=x_3} + \frac{V_{in}}{LC}k_{dc}(t)$$

According to the ADRC theory $\ddot{v}(t) = f(t) + \frac{V_{in}}{LC}k_{dc}(t)$, and its state dynamics will be:

$$\begin{aligned} \dot{x}_1 &= x_2 \\ \dot{x}_2 &= x_3 + \frac{V_{in}}{LC}k_{dc}(t) \\ \dot{x}_3 &= \dot{f}(t) = w(t) \end{aligned} \tag{42}$$

Open-loop analysis of the buck converter indicates that the settling time of the converter is 862.6 µs. The control law for the converter is designed to operate at a settling time of 250 µs to have faster convergence. This implies that the dominant pole of the control should be placed at $s_{\text{dominat}} = s_1 = -\zeta\omega_n \cong 4/\left(250 \times 10^{-6}\right) = -4 \times 10^3$, while the second pole is placed 25-times deeper into the negative s-plane, $s_2 = -1 \times 10^5$. The closed-loop characteristic equation of the converter system will be $s^2 + 1.04 \times 10^5 s + 4 \times 10^8 = 0$. Now, comparing the parameters of control law in (31) with the coefficient of this characteristic equation, the values of $c_1$ and $k_1$ are found to be $c_1 = 4 \times 10^3$ and $k_1 = 4 \times 10^5$. The control law is based on the smooth switching function (described in Definition 1) with $a_\phi = 1$, $b_\phi = 1$, gain of $\epsilon = 10$, and $\mu = 0.05$.

The closed-loop control system of the converter is shown in Figure 6, while the step response of the converter with the control system design above is shown in Figure 7. The converter's response indicates that the control system is operating as desired. Detailed performance analysis of the converter will be described in the next section.

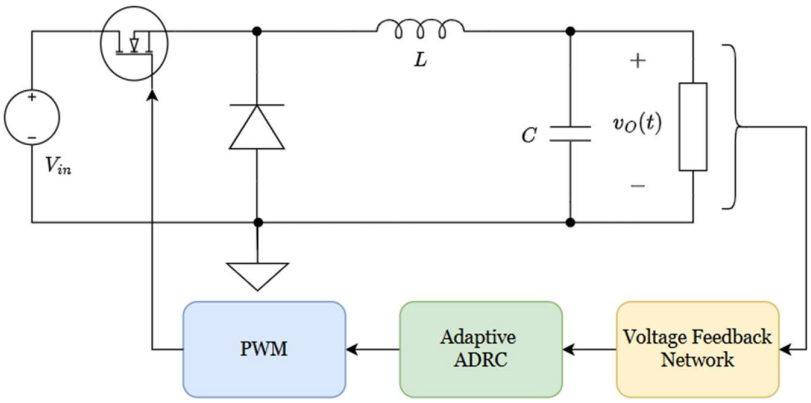



**Figure 6.** Buck converter closed-loop ADRC system.

The design of adaptive ESO based on the settling is much lower than the settling time of the closed-loop system. The settling time of the ESO is set at $t_s = 25$ µs. Therefore, the parameters of the ESO are $\left(s + 4/\left(25 \times 10^{-6}\right)\right)^3 = s^3 + 4.8 \times 10^5 s^2 + 7.68 \times 10^{10} s + 4.096 \times 10^{15} = 0$. A smooth scaling function $\varphi\left(\tilde{x}_1\right)$ is also part of the observer, and its selection parameters are $a_\varphi = 0.75$, $b_\varphi = 1.05$, and $\mu = 0.05$.

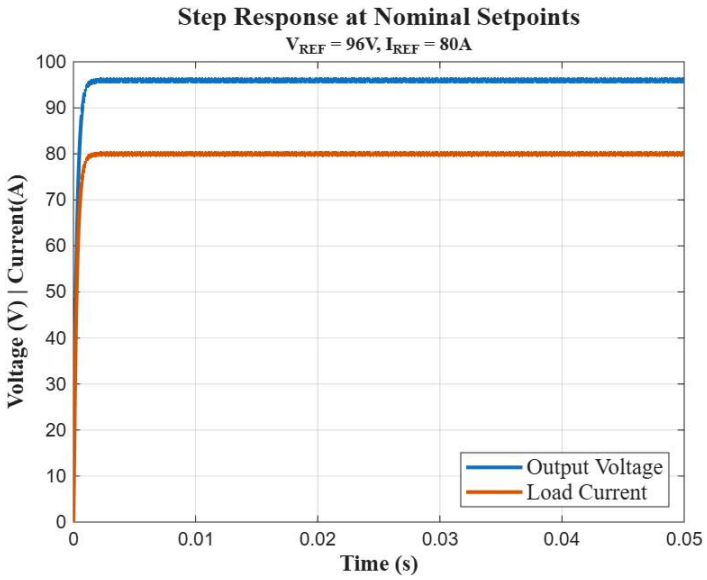



**Figure 7.** Step response of the buck converter.

3.2.2. Adaptive ADRC Design and Implementation for Boost Converter

Like the buck converter circuit, it is also designed to deliver a power of 7.6 kW at a switching frequency of 100 kHz. The input voltage to the converter is 96 V, and the required output from the converter is 380 V. Design specifications, the resulting filtering (inductor and capacitor), and switching components (MOSFET and diode) are listed in Table 2. The transfer function of the converter is described as:

$$G_{boost}(s) = \frac{V_O(s)}{k_{dc}(s)} = \frac{\frac{V_{in}}{LC}\left(-\frac{L}{R(1-k_{\mathrm{DC}})^2}s + 1\right)}{s^2 + \frac{1}{RC}s + \frac{(1-k_{\mathrm{DC}})^2}{LC}} \implies$$

$$\ddot{v}(t) = \underbrace{-\frac{1}{RC}\dot{v}(t) - \frac{(1-k_{\mathrm{DC}})^2}{LC}v(t) - \frac{V_{in}}{RC(1-k_{\mathrm{DC}})^2}\frac{dk_{dc}(t)}{dt}}_{f(t)=x_3(t)} + \frac{V_{in}}{LC}k_{dc}(t)$$

Thus, according to the ADRC theory $\ddot{v}(t) = f(t) + \frac{V_{in}}{LC}k_{dc}(t)$, and its state dynamics will be:

$$\begin{aligned} \dot{x}_1 &= x_2 \\ \dot{x}_2 &= x_3 + \tfrac{V_{in}}{LC}k_{dc}(t) \\ \dot{x}_3 &= \dot{f}(t) = w(t) \end{aligned} \tag{43}$$

Open-loop analysis of the boost converter indicates that the settling time of the converter is 266.5 ms. The control law for the converter is designed to operate at a settling time of 16 ms. This implies that the dominant pole of the control should be placed at $s_{\text{dominat}} = s_1 = -\zeta\omega_n \cong 4/16 \times 10^{-3} = -250$, while the second pole is placed 10-times deeper into the negative s-plane from the dominant pole, $s_2 = -2500$. The closed-loop characteristic equation of the converter system will be $s^2 + 2750s + 6.25 \times 10^5 = 0$. Now, comparing the parameters of the control law in (31) with the coefficient of this characteristic equation, the values of $c_1$ and $k_1$ are found to be $c_1 = 250$ and $k_1 = 2500$. The control law is based on a smooth switching function (described in Definition 1) with $a_\phi = 1$, $b_\phi = 2$, a gain of $\epsilon = 10$, and $\mu = 0.05$.

The design of adaptive ESO based on the settling is much lower than the settling time of the open-loop system. This helps quickly mitigate the effects of the converter's zero that

lies in the right half of the s-plane and other unknown disturbances. The settling time of the ESO is set at $t_s = 160$ µs. Therefore, the parameters of the ESO are $\left(s + 4/\left(160 \times 10^{-6}\right)\right)^3 = s^3 + 7.5 \times 10^4 s^2 + 1.875 \times 10^9 s + 1.5625 \times 10^{13} = 0$. A smooth scaling function $\varphi\left(\tilde{x}_1\right)$ is also part of the observer, and its selection parameters are $a_\varphi = 0.75$, $b_\varphi = 1.05$, and $\mu = 0.05$.

The closed-loop implementation of the converter is shown in Figure 8, while its step response is shown in Figure 9. The results in Figure 9 demonstrate that the converter converges to stable response as the design implementation dictates, without any overshoots.

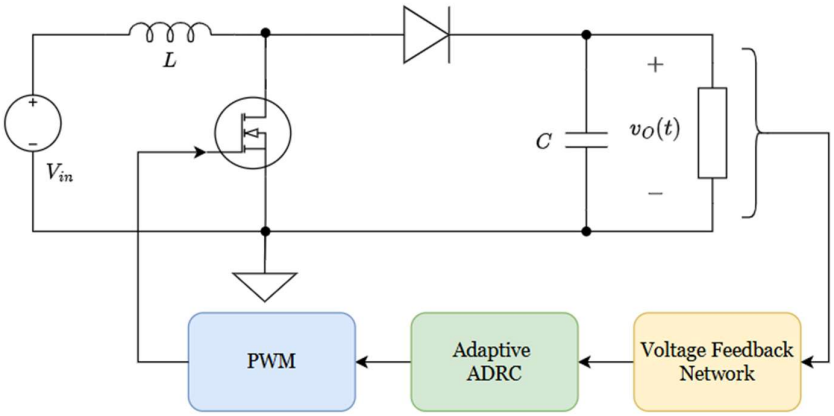



**Figure 8.** ADRC closed-loop system for boost converter.

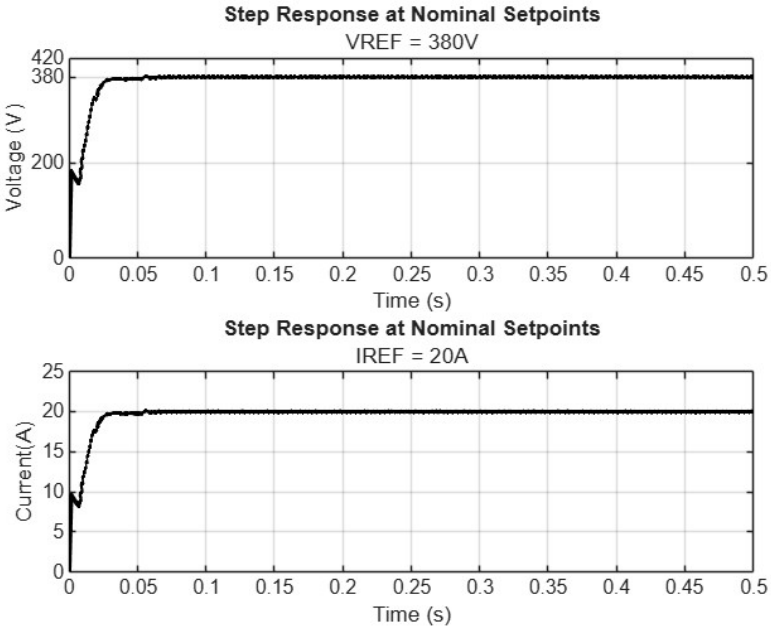



**Figure 9.** Step response of boost converter control system.

### 3.2.3. Adaptive ADRC Design and Implementation for Single-Phase Inverter

The design of the single-phase inverter is based on the buck converter presented previously, with small changes. The design of the converter is accomplished using a switching frequency of 10 kHz, while the output voltage is set to 230 V RMS against the input voltage of 380 V DC. The controller design is accomplished like the ADRC controller design for the buck converter, in a way that the controller does not need to regulate the sinusoidal output voltage, but it needs to regulate the RMS of the output voltage.

The closed-loop ADRC implementation of the converter using unipolar sinusoidal PWM (UP-SPWM) is shown in Figure 10, while its step response inverter is shown in

Figure 11. The adaptive ADRC as proposed in this work successfully controls the response of the inverter at the desired AC frequency of 50 Hz.

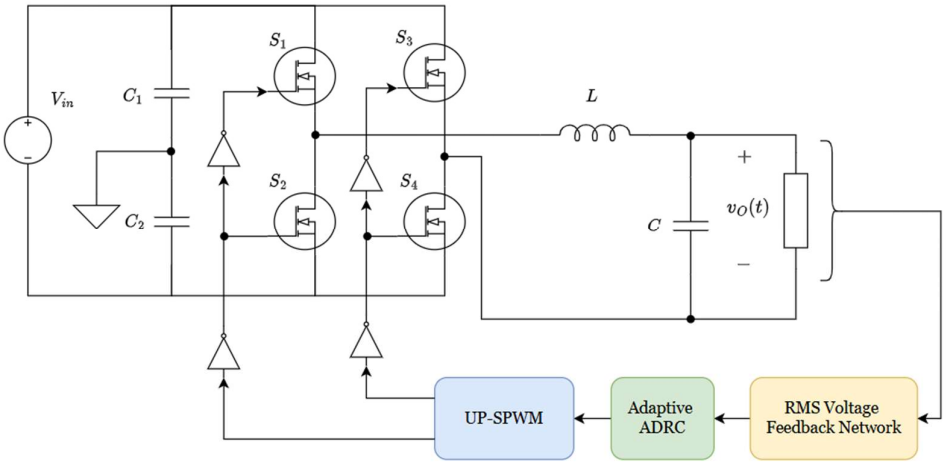



**Figure 10.** ADRC closed-loop implementation for single-phase inverter.

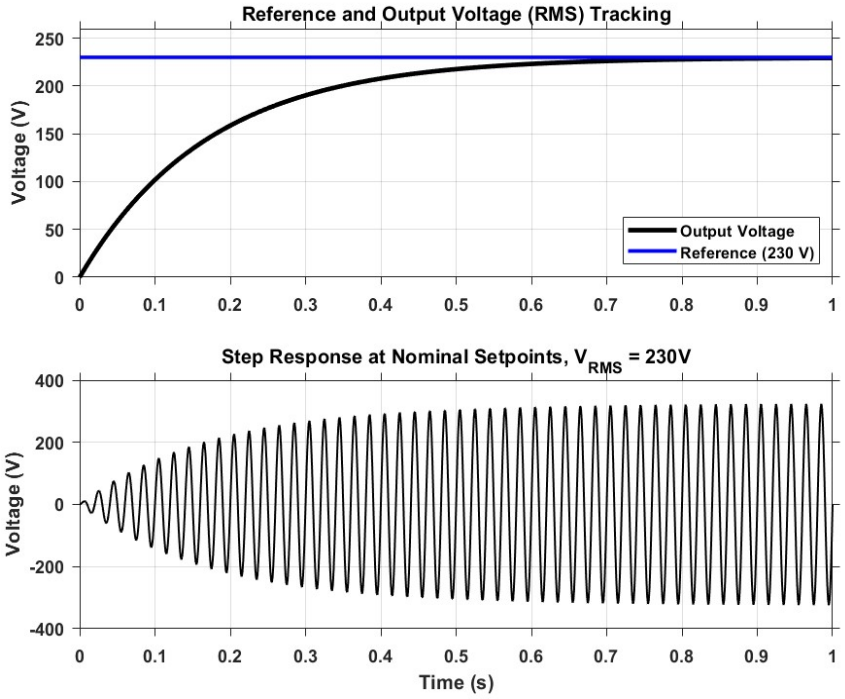



**Figure 11.** Step response of single-phase inverter.

## 4. Results and Discussion

The following section presents a detailed evaluation of the proposed adaptive ADRC framework applied to buck, boost, and single-phase inverter converters. Simulation results are generated to demonstrate the controller's ability to achieve faster dynamic response, strong disturbance rejection, and robust performance under wide operating conditions. These key characteristics are gauged using reference tracking, line regulation, and load regulation. The results of the adaptive ADRC will be compared with classic PI control and linear ADRC. These findings validate the effectiveness of the proposed control strategy and highlight its advantages over conventional approaches.

### *4.1. Performance Analysis of Buck Converter*

As described earlier, the performance of the converter is gauged using reference tracking signal, line regulation, and load regulation. Figure 12 illustrates the tracking performance of the converter in comparison to PI control and LADRC. In this Figure, subfigure (a) represents the reference voltage and current signal, (b) represents the adaptive ADRC response to reference voltage, (c) represents the response of the ADRC to reference, and (d) represents the PI controller response to the changing reference voltage signal. The reference-tracking performance of AADRC is excellent since it presents the slightest fluctuations in the desired output voltage without compromising on the required load current. Throughout the 3 s simulation, the reference signal undergoes multiple changes while the reference load current is maintained at 60 A. The converter's control system, based on the adaptive ADRC strategy, consistently ensures accurate tracking of the reference voltage.

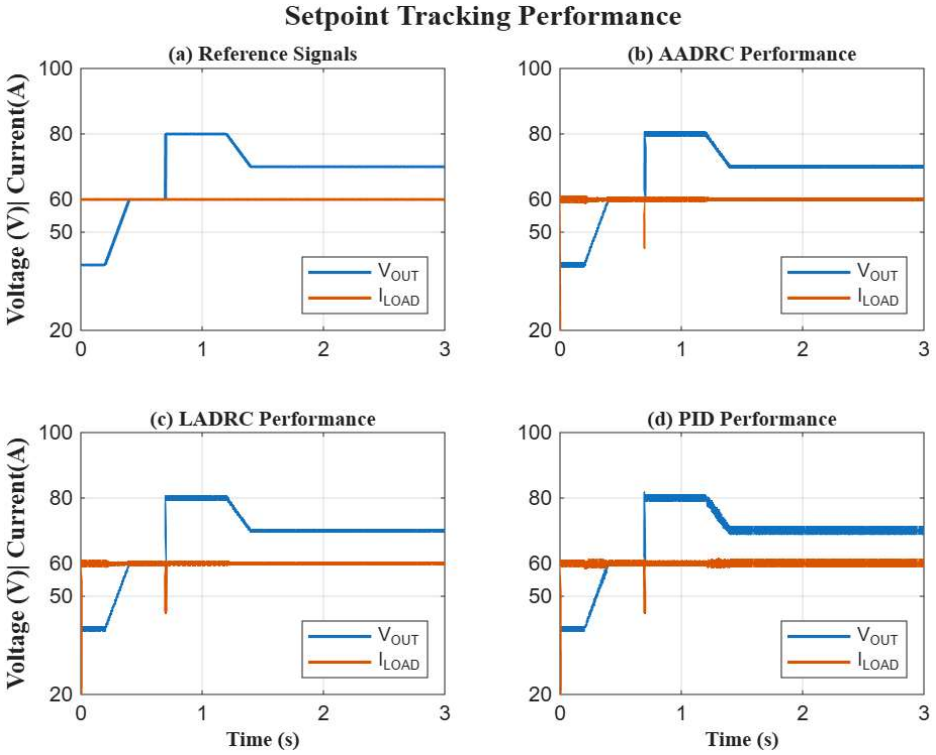



**Figure 12.** Tracking performance of the buck converter closed-loop system.

At t = 0.8 s, the reference voltage signal changes from 60 V to 80. All controllers successfully tracked the required voltage, but with a sudden jump in current. The results are looked at closely, and the output voltage from the PI-controlled converter does exhibit small fluctuations in the output voltage.

Figure 13 illustrates the line-regulation capability of the converter under significant input-voltage disturbances. The input voltage is intentionally varied sinusoidally by ±30 V around the nominal 380 V at a frequency of 10 Hz to emulate severe line fluctuations. Throughout this test, the reference output voltage is maintained at 96 V, and the load current is fixed at 80 A. Despite the substantial and continuous variations in the input voltage, the converter preserves a stable output voltage of 96 V and sustains the desired load current of 80 A. A comparison of these results with PI and LADRC can also be seen. Both AADRC and LADRC perform better than PI controllers. Using cursor measurement, it has been found that the linear regulations of AADRC and LADRC are 0.7% and 1.3%, respectively, while the line regulation of the PI-controlled converter is 3.5%. These results demonstrate

AADRC's strong disturbance-rejection capability and confirm that the converter effectively rejects input-side fluctuations, maintaining robust line regulation.

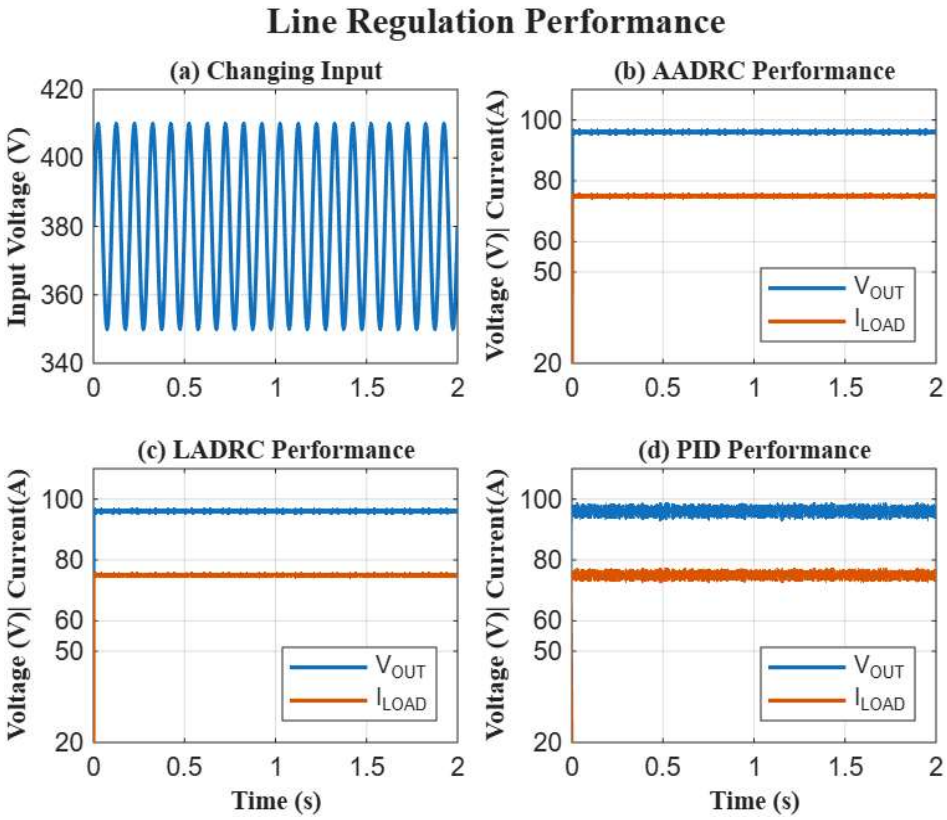



**Figure 13.** Line-regulation performance for buck converter control system.

Figure 14 presents the load-regulation performance of the converter under dynamic load variations in comparison with LADRC and PI-controlled buck converters. During the 3 s simulation, the load current is intentionally varied multiple times to evaluate the controller's ability to maintain stable operation. Throughout this test, the reference output voltage is fixed at 96 V. Despite the repeated and abrupt changes in load current, the converter maintains the output voltage at the desired 96 V and accurately tracks the commanded load-current profile. This demonstrates strong load-regulation capability, confirming that the control system effectively rejects load-side disturbances and preserves stable output behavior. Using cursor measurement, the load regulation of the PI-controlled converter is computed to be 9.38%, while AADRC and LADRC exhibit a line regulation of 1.56% and 1.042%.

The adaptive ADRC controller delivers consistently strong performance for the buck converter across reference-tracking, line-regulation, and load-regulation tests. It accurately follows time-varying voltage references—including multiple step and ramp transitions—while maintaining stable output behavior and negligible steady-state error. Under input-voltage disturbances of roughly ±30 V around the nominal value, the controller effectively rejects line variations and preserves tight regulation of the output voltage. When subjected to stepped–ramped load-current changes around the nominal 80 A, the converter maintains stable operation and holds the output voltage close to its reference without overshoot or oscillation. Overall, the adaptive ADRC demonstrates robust disturbance rejection, fast dynamic response, and reliable voltage regulation under diverse operating conditions.

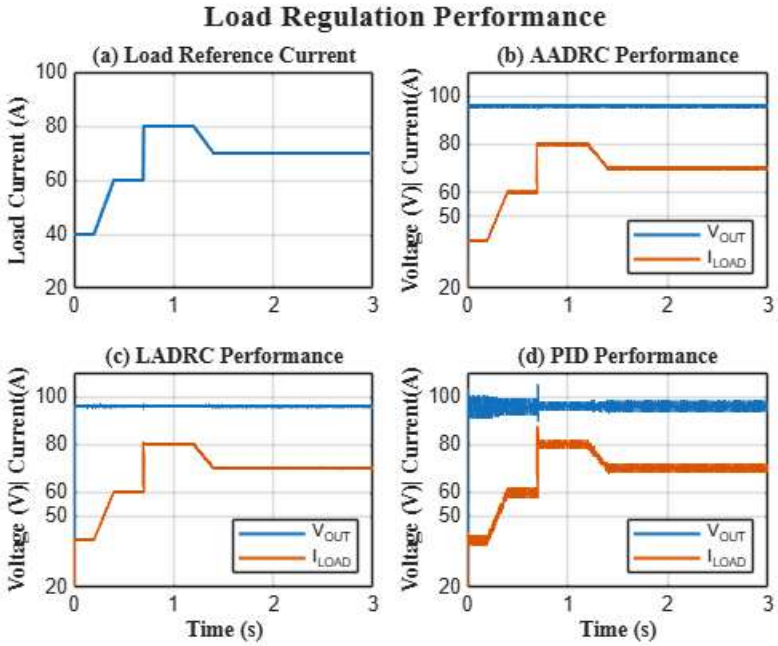



**Figure 14.** Load-regulation performance for buck converter control system.

*4.2. Performance Analysis of Boost Converter*

Like the buck converter, its performance is also evaluated using reference tracking, line regulation, and load regulation. The dynamic reference-tracking capability of the proposed control scheme is evaluated on a boost converter operating with a constant load current of 20 A. As shown in Figure 15, during this test, the output-voltage reference is intentionally varied multiple times using a combination of step and ramp changes to emulate realistic operating conditions. Specifically, the reference signal steps to 350 V at 0 s, then it ramps from 350 V to 400 V during $t = 1$ s to $t = 2$ s and stays there by $t = 3$ s. At $t = 3$s, it ramps down to 380 V in 0.5 s and stays there for the rest of the simulation time. Throughout these variations, the control system continuously adjusts the duty cycle to regulate the inductor current and output voltage.

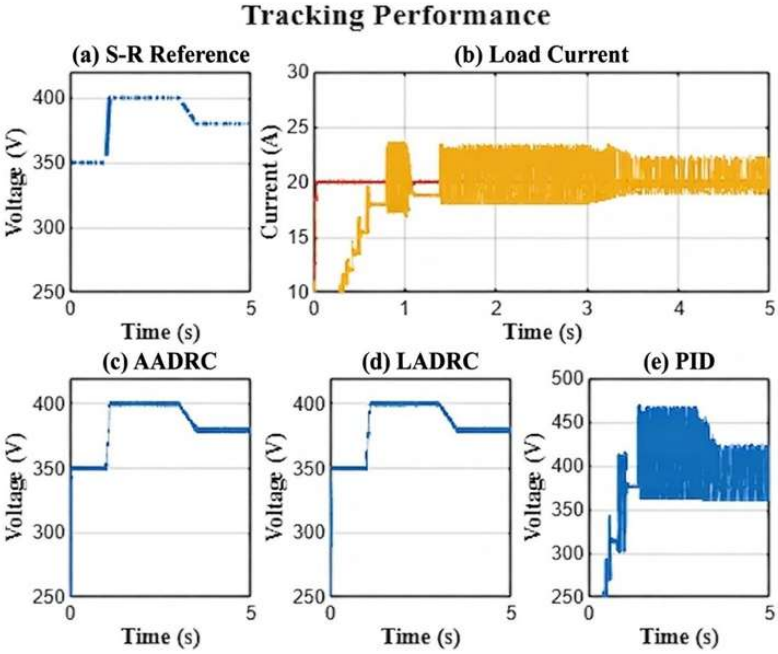



**Figure 15.** Reference tracking performance of boost converter system.

The results in Figure 15 show that the converter output voltage closely follows the changing reference trajectory with negligible steady-state error and fast transient response. Both step changes and ramp segments are accurately tracked without an overshoot large enough to compromise performance or stability. Importantly, despite the aggressive reference variations, the load current remains tightly regulated around 20 A, demonstrating that the controller effectively decouples output-voltage tracking from load-current regulation. This confirms the robustness and tracking capability of the proposed control strategy under time-varying reference commands.

The line-regulation capability of the boost converter is assessed by subjecting the input voltage to a ±20% variation around its nominal value of 96 V, as shown in Figure 16. This test emulates realistic supply disturbances by introducing both upward and downward deviations in the input line while maintaining the output-voltage reference at 380 V and the load-current reference at 20 A. Despite these significant input-side perturbations, the proposed control system preserves stable operation and effectively rejects the line disturbances. The output voltage remains tightly regulated around its reference with negligible deviation, and no noticeable degradation in transient behavior is observed during the input-voltage excursions. Furthermore, the load current stays consistently controlled at 20 A, demonstrating that the controller successfully isolates the output dynamics from input-side fluctuations. These results confirm the robustness of the control strategy and its strong capability to maintain regulation under varying supply conditions.

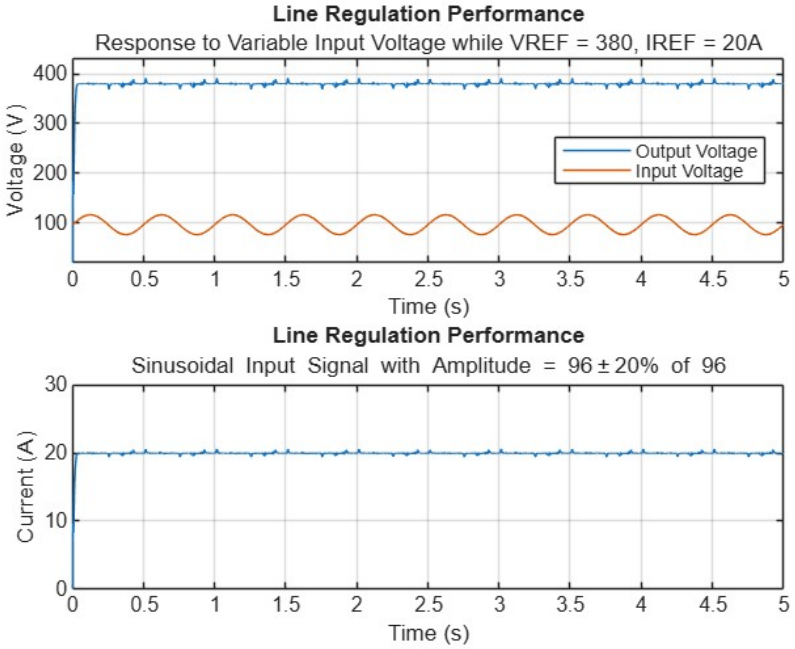



**Figure 16.** Line regulation for boost converter system.

The load-regulation performance of the boost converter is evaluated using a stepped–ramped load-current profile centered around 20 A, as detailed in Figure 17. With the input voltage fixed at 96 V and the output-voltage reference held at 380 V, the test introduces both abrupt and gradual variations in the demanded load current to assess disturbance-rejection capability. Throughout the sequence of step changes and ramp transitions, the converter maintains tight voltage regulation with minimal deviation from the reference. The controller responds rapidly to sudden load disturbances and smoothly compensates for ramped variations without overshoot or oscillatory behavior. Despite the imposed load dynamics, system stability is preserved, and the voltage-regulation loop effectively isolates the output from load-side fluctuations. These results confirm the robustness of

the control strategy and its ability to sustain accurate voltage regulation under dynamic load conditions.

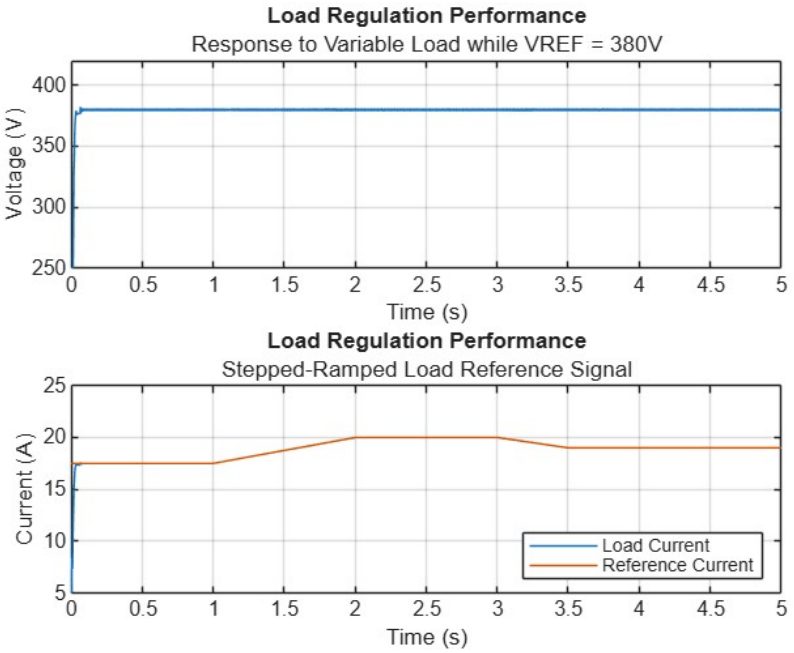



**Figure 17.** Load regulation of boost converter system.

The combined results from the reference-tracking, line-regulation, and load-regulation tests demonstrate the strong dynamic and steady-state performance of the boost converter's control system under a wide range of operating conditions. The controller accurately follows time-varying voltage references, including multiple step-and-ramp transitions, while maintaining a constant 20 A load current. It also effectively rejects ±20% input-voltage disturbances around the nominal 96 V level, preserving tight regulation of the 380 V output. Finally, under stepped–ramped load-current variations, the converter sustains stable operation and maintains the output voltage with minimal deviation. Collectively, these results confirm the robustness, disturbance-rejection capability, and high-quality regulation achieved by the proposed control strategy across reference, line, and load variations.

### *4.3. Performance Analysis of Single-Phase Inverter*

This subsection presents the performance of an adaptively controlled single-phase system using ADRC under different test conditions. Theoretical proofs of the proposed control scheme using well-established Lyapunov stability theory, singular perturbation theory, and input-to-state stability theory have established the effectiveness of adaptive ADRC. Here, the same is proved using numerical simulations.

The performance of the adaptive ADRC controller for the single-phase inverter is evaluated under a stepped RMS-voltage reference profile, designed to test its dynamic tracking capability. The reference is initially set to 180 VRMS for the first 2 s and then increased to 230 VRMS for the remaining interval up to 5 s. This abrupt change introduces a significant disturbance that challenges both the voltage-regulation loop and the disturbance-rejection mechanism. The reference and output signals, RMS output voltage, and AC output voltage are shown in Figure 18.

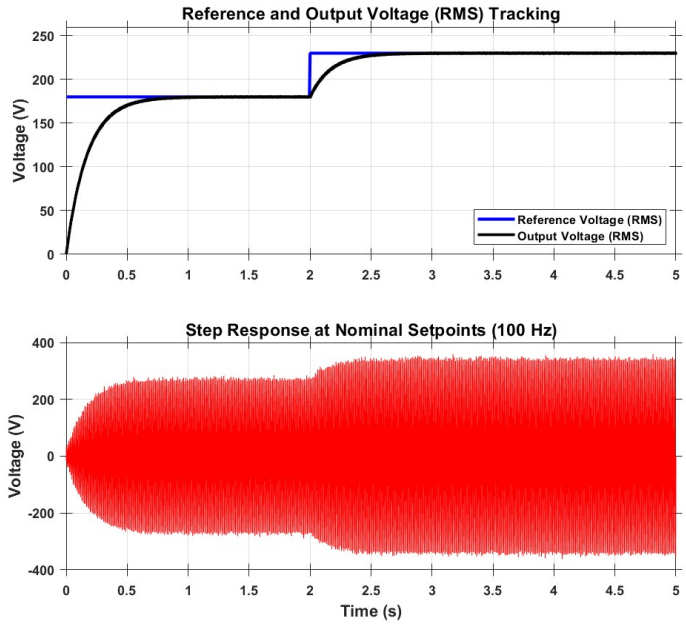



**Figure 18.** Inverter response to varying step RMS voltage references.

As shown throughout the entire test, the adaptive ADRC maintains excellent tracking performance. During the first interval, the inverter output rapidly settles to 180 VRMS reference with minimal overshoot and negligible steady-state error. When the reference steps to 230 VRMS, the controller responds promptly, adjusting the control effort to achieve the new target without oscillations or instability. The embedded extended state observer effectively compensates for model uncertainties and load-side disturbances, ensuring smooth transitions between reference levels. Overall, the results confirm that the adaptive ADRC provides robust, accurate, and fast reference tracking under stepped RMS-voltage commands, demonstrating strong suitability for dynamic inverter applications.

The adaptive ADRC controller is further evaluated under a highly nonlinear loading condition by connecting a diode-bridge rectifier at the inverter output. The voltage waveforms at the inverter terminals and rectifier load terminal are shown in Figure 19. This load introduces strong harmonic distortion, discontinuous current, and rapid waveform changes that typically degrade voltage quality. Despite these challenges, the controller maintains excellent regulation of the output at 230 VRMS. The extended state observer effectively estimates and compensates for the disturbances generated by the rectifier, allowing the inverter to preserve a stable fundamental voltage with minimal deviation. No oscillations or instability are observed, and the system responds smoothly to the distorted load current. These results highlight the robustness of the adaptive ADRC in sustaining high-quality voltage regulation under severe nonlinear load conditions.

The adaptive ADRC controller delivers strong and reliable performance for the single-phase inverter across all tested conditions. It accurately tracks stepped RMS-voltage references, transitioning smoothly from 180 VRMS to 230 VRMS with fast settling and minimal error. Under nonlinear loading, including a diode-bridge rectifier, the controller maintains a stable 230 VRMS output despite a distorted and discontinuous current. Its extended state observer effectively compensates for uncertainties and load-induced disturbances, ensuring clean voltage regulation and robust dynamic response. Overall, the adaptive ADRC demonstrates excellent tracking, disturbance rejection, and stability, confirming its suitability for demanding inverter applications.

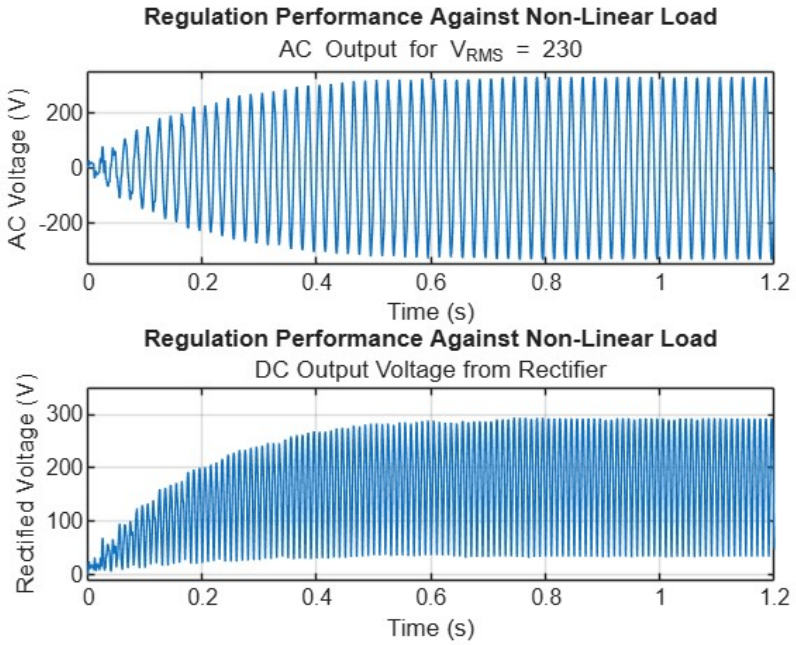



**Figure 19.** Performance against nonlinear load.

## 5. Conclusions and Future Recommendations

### *5.1. Conclusive Remarks*

This study is set out to develop and evaluate an adaptive active disturbance rejection control framework that enhances voltage and current regulation in power-electronic converters. The work focused on addressing the limitations of conventional ADRC by introducing a customizable error-scaled ESO- and an SMC-inspired control law (designed using a smooth switching function) capable of improving robustness while diminishing chattering.

Across the three tested converter platforms, the buck converter, boost converter, and the proposed controller consistently achieved accurate reference tracking, strong rejection of input-voltage disturbances, and stable performance under dynamic and nonlinear load conditions. These outcomes directly confirm that the adaptive mechanism and customizable structures significantly strengthen disturbance estimation and control precision. In the broader context of power-electronics control, the findings demonstrate that ADRC can be made more flexible, smoother in operation, and better suited for systems with rapidly changing operating points.

The study contributes a methodological advancement by showing how tailored observer scaling and smooth switching functions can be integrated into ADRC without sacrificing stability. While the work is primarily simulation-based and limited to selected converter topologies, it provides a solid foundation for future experimental and large-scale validation.

Overall, the research highlights the potential of adaptive ADRC as a robust and versatile control solution for modern power-conversion systems, offering a promising direction for both academic development and practical deployment.

### *5.2. Future Recommendations*

Building on the findings and acknowledging the scope of this study, several directions emerge for advancing research on adaptive ADRC in power-electronic systems. Future work should investigate how the proposed error-scaled ESO and smooth switching function perform under a wider range of converter topologies, grid-connected environments, and high-power industrial conditions. This research uses symmetric scaling and smoothing functions. Particularly, future research should explore whether the non-symmetric scaling

and smoothing functions can contribute to better ADRC frameworks. Exploring such adaptive mechanisms would further enhance the applicability of ADRC against parameter drifts, component aging, and thermal effects.

Methodologically, experimental validation on hardware prototypes, larger test sets, and long-duration stress testing would help verify the controller's robustness beyond simulation. Comparative studies using alternative control architectures or hybrid designs could also clarify the boundaries of the proposed method.

From a theoretical perspective, integrating the adaptive ADRC framework with modern learning-based tuning strategies or embedding it within broader nonlinear control theories may reveal deeper insights into disturbance-estimation behavior. Testing the controller within different theoretical models—such as passivity-based control or predictive control—could broaden its conceptual grounding.

Practically, the approach may benefit industries seeking smoother, more resilient regulation in renewable-energy converters, electric-vehicle chargers, and distributed power systems. Evaluating performance across different regions, load profiles, and mission conditions would support broader generalization.

Finally, emerging trends such as digital-twin platforms, high-speed embedded processors, and data-driven observers offer promising tools for extending and refining this line of research.

**Author Contributions:** Conceptualization, G.S., A.H., M.Y.J., A.B.A. and T.M.; methodology, G.S., A.H. and M.Y.J.; writing—original draft preparation, G.S. and M.Y.J.; writing—review and editing, G.S., A.H., M.Y.J., A.B.A. and T.M.; resources, G.S., A.H., M.Y.J. and T.M.; supervision, M.Y.J., A.B.A. and T.M.; project administration, G.S., A.H. and M.Y.J. All authors have read and agreed to the published version of the manuscript.

**Funding:** This research received no external funding.

**Data Availability Statement:** No specific available datasets were used in this study. All the results reported in the paper are based on simulation experiments performed on MATLAB/Simulink (R2025b) models.

**Conflicts of Interest:** The authors declare no conflicts of interest.

## Abbreviations

| | |
|---|---|
| ADRC | Active disturbance rejection control |
| AESO | Adaptive extended state observer |
| DC-ESO | Disturbance-compression extended state observer |
| EHGO | Extended high-gain observer |
| ESO | Extended state observer |
| FO-ADRC | Fractional-order active disturbance rejection control |
| FTCL | Finite-time convergent control |
| FTESO | Finite-time extended state observer |
| FXTESO | Fixed-time extended state observer |
| HGESO | High-gain extended state observer |
| INTD | Improved nonlinear tracking differentiator |
| ISS | Input-to-state stability |
| LADRC | Linear active disturbance rejection control |
| LESO | Linear extended state observer |
| LST | Lyapunov stability theory |
| MIMO | Multiple-input multiple-output |
| NESO | Nonlinear extended state observer |
| PI | Proportional–integral |

| | |
|---|---|
| PID | Proportional–integral–derivative |
| PR | Proportional–resonant |
| RESO | Reduced-order extended state observer |
| RMS | Root mean square |
| SMC | Sliding-mode control |
| SPT | Singular perturbation theory |
| TD | Tracking differentiator |
| UP-SPWM | Unipolar sinusoidal pulse width modulation |

## References


1. Hu, J.; Shan, Y.; Cheng, K.W.; Islam, S. Overview of Power Converter Control in Microgrids—Challenges, Advances, and Future Trends. *IEEE Trans. Power Electron.* **2022**, *37*, 9907–9922. [CrossRef]
2. Ghamari, S.M.; Khavari, F.; Mollaee, H. Lyapunov-based adaptive PID controller design for buck converter. *Soft Comput.* **2023**, *27*, 5741–5750. [CrossRef]
3. Xu, L.; Zhuo, S.; Liu, J.; Jin, S.; Huangfu, Y.; Gao, F. Advancement of Active Disturbance Rejection Control and Its Applications in Power Electronics. *IEEE Trans. Ind. Appl.* **2024**, *60*, 1680–1694. [CrossRef]
4. Aliamooei-Lakeh, H.; Aliamooei-Lakeh, S.; Toulabi, M.; Amraee, T. Enhancement in Robust Performance of Boost Converter-Based Distributed Generations Utilizing Active Disturbance Rejection Controller. *IEEE Trans. Autom. Sci. Eng.* **2024**, *21*, 6094–6108. [CrossRef]
5. Herbst, G.; Madonski, R. *Active Disturbance Rejection Control*; Springer Nature: Cham, Switzerland, 2025. [CrossRef]
6. Khadraoui, S.; Fareh, R.; Baziyad, M.; Elbeltagy, M.B.; Bettayeb, M. A Comprehensive Review and Applications of Active Disturbance Rejection Control for Unmanned Aerial Vehicles. *IEEE Access* **2024**, *12*, 185851–185868. [CrossRef]
7. Ye, J.; Guo, J.; Hao, F. Stability Analysis of Linear Active Disturbance Rejection Control. In Proceedings of the 2024 IEEE International Conference on Control Science and Systems Engineering, ICCSSE 2024, Beijing, China, 18–20 October 2024; pp. 25–31. [CrossRef]
8. Marconi, L. Regulation and Tracking of Nonlinear Systems. In *Encyclopedia of Systems and Control*; Springer: Cham, Switzerland, 2021; pp. 1845–1850. [CrossRef]
9. Nikiforov, V.; Gerasimov, D. *Adaptive Regulation*; Springer: Cham, Switzerland, 2022; Volume 491. [CrossRef]
10. Wang, X.; Yang, J.; Liu, C.; Yan, Y.; Li, S. Safety-Critical Disturbance Rejection Control of Nonlinear Systems with Unmatched Disturbances. *IEEE Trans. Automat. Contr.* **2025**, *70*, 2722–2729. [CrossRef]
11. Li, P.; Duan, G. High-Order Fully Actuated Control Approaches of Flexible Servo Systems Based on Singular Perturbation Theory. *IEEE/ASME Trans. Mechatron.* **2023**, *28*, 3386–3397. [CrossRef]
12. He, K.; Dong, C.; Wang, Q. Active Disturbance Rejection Control for Uncertain Nonlinear Systems with Sporadic Measurements. *IEEE/CAA J. Autom. Sin.* **2022**, *9*, 893–906. [CrossRef]
13. Liu, H.; Liu, W. Active Disturbance Rejection Tajectory Tracking Control of a Delta Robot Based on LMI. In Proceedings of the 2024 International Annual Conference on Complex Systems and Intelligent Science, CSIS-IAC 2024, Guangzhou, China, 20–22 September 2024; pp. 145–150. [CrossRef]
14. Zhang, X.; Lang, P.H. Tracking Differentiators for Both the Real Time Signals and the Time Delayed Signals. *IEEE Access* **2024**, *12*, 113910–113917. [CrossRef]
15. Yang, X.; Huang, Q.; Jing, S.; Zhang, M.; Zuo, Z.; Wang, S. Servo system control of satcom on the move based on improved ADRC controller. *Energy Rep.* **2022**, *8*, 1062–1070. [CrossRef]
16. Liu, J.; Ni, K.; Shan, H.; Fan, M.; Yang, Y.; Hu, Y. An Improved Sensorless Control Method for PMSMs with High Anti-Disturbance Ability Based on Sliding Mode Observer Super-Twisting Algorithm. In Proceedings of the 2025 IEEE 12th International Symposium on Sensorless Control for Electrical Drives (SLED), Harbin, China, 15–17 August 2025; pp. 1–6. [CrossRef]
17. Li, J.; Zhuang, S.; Wang, H.; Deng, J.; Mao, Y. Design of Backstepping Control Based on a Softsign Linear–Nonlinear Tracking Differentiator for an Electro-Optical Tracking System. *Photonics* **2024**, *11*, 156. [CrossRef]
18. Kasim, I.; Riyadh, W. On the Improved Nonlinear Tracking Differentiator based Nonlinear PID Controller Design. *Int. J. Adv. Comput. Sci. Appl.* **2016**, *7*. [CrossRef]
19. Hu, K.; Niu, J.; Jiang, Q.; Yang, J.; Zhang, W. Magnetic levitation system control based on a novel tracking differentiator. *ISA Trans.* **2024**, *151*, 350–362. [CrossRef] [PubMed]
20. Marwan, H.; Humaidi, A.J.; Al-Khazraji, H. Active Disturbance Rejection Control for Unmanned Aerial Vehicle. *Int. J. Robot. Control. Syst.* **2025**, *5*, 1278–1296. [CrossRef]
21. Qin, B.; Yan, H.; Wang, M.; Rao, K.; Yang, P. Nolinear tracking differentiator based practical prescribed time tracking control for perturbed wheeled mobile robot. *Nonlinear Dyn.* **2024**, *113*, 1389–1400. [CrossRef]

22. Song, C.; Du, Q.; Yang, S.; Feng, H.; Pang, H.; Li, C. Flexible joint parameters identification method based on improved tracking differentiator and adaptive differential evolution. *Rev. Sci. Instrum.* **2022**, *93*, 084706. [CrossRef] [PubMed]
23. Zhang, J.; Cui, C.; Gu, S.; Wang, T.; Zhao, L. Trajectory Tracking Control of Pneumatic Servo System: A Variable Gain ADRC Approach. *IEEE Trans. Cybern.* **2023**, *53*, 6977–6986. [CrossRef]
24. Abdul-Adheem, W.R.; Ibraheem, I.K.; Humaidi, A.J.; Alkhayyat, A.; Maher, R.A.; Abdulkareem, A.I.; Azar, A.T. Design and Analysis of a Novel Generalized Continuous Tracking Differentiator. *Ain Shams Eng. J.* **2022**, *13*, 101656. [CrossRef]
25. Gong, Y.; Guo, Y.; Li, D.; Ma, G.; Ran, G. Predefined-time tracking control for high-order nonlinear systems with control saturation. *Int. J. Robust Nonlinear Control* **2022**, *32*, 6218–6235. [CrossRef]
26. Stankovic, M.; Ting, H.; Madonski, R. From PID to ADRC and back: Expressing error-based active disturbance rejection control schemes as standard industrial 1DOF and 2DOF controllers. *Asian J. Control* **2024**, *26*, 2796–2806. [CrossRef]
27. Han, J. From PID to Active Disturbance Rejection Control. *IEEE Trans. Ind. Electron.* **2009**, *56*, 900–906. [CrossRef]
28. Du, Y.; Cao, W.; She, J. Analysis and Design of Active Disturbance Rejection Control with an Improved Extended State Observer for Systems with Measurement Noise. *IEEE Trans. Ind. Electron.* **2023**, *70*, 855–865. [CrossRef]
29. Chi, R.; Guo, X.; Lin, N.; Huang, B. Dynamic Linearization and Extended State Observer-Based Data-Driven Adaptive Control. *IEEE Trans. Syst. Man Cybern. Syst.* **2023**, *53*, 6805–6814. [CrossRef]
30. Herbst, G. A Simulative Study on Active Disturbance Rejection Control (ADRC) as a Control Tool for Practitioners. *Electronics* **2013**, *2*, 246–279. [CrossRef]
31. Fu, R. Model-Free Predictive Current and Speed Control with Ultralocal Model for PMSM Drives Using Exponential High-Gain Extended State Observer. *IEEE J. Emerg. Sel. Top. Power Electron.* **2025**, *13*, 6099–6108. [CrossRef]
32. Won, D.; Kim, W.; Tomizuka, M. Nonlinear Control with High-Gain Extended State Observer for Position Tracking of Electro-Hydraulic Systems. *IEEE/ASME Trans. Mechatron.* **2020**, *25*, 2610–2621. [CrossRef]
33. Ji, Y.; Xu, Z.; Liu, J.; Song, Y. Distributed Extended High-Gain Observers for the Generalized Strict-Feedback System. *Int. J. Robust Nonlinear Control* **2023**, *33*, 7649–7666. [CrossRef]
34. Patelski, R.; Pazderski, D.; Patelski, R.; Pazderski, D. Novel Adaptive Extended State Observer for Dynamic Parameter Identification with Asymptotic Convergence. *Energies* **2022**, *15*, 3602. [CrossRef]
35. Liu, W.; Wu, G. Automatic clutch control using ADRC with continuous adaptive extended state observer. *Int. J. Robust Nonlinear Control* **2025**, *35*, 82–101. [CrossRef]
36. Shen, H.; Zhou, X.; Wang, Z.; Wang, J. State of charge estimation for lithium-ion battery using Transformer with immersion and invariance adaptive observer. *J. Energy Storage* **2022**, *45*, 103768. [CrossRef]
37. Zhao, J.; Feng, D.; Cui, J.; Wang, X. Finite-Time Extended State Observer-Based Fixed-Time Attitude Control for Hypersonic Vehicles. *Mathematics* **2022**, *10*, 3162. [CrossRef]
38. Lu, H.; Li, J.; Li, S.; Wang, S.; Xiao, Y. Finite-time extended state observer enhanced nonsingular terminal sliding mode control for buck converters in the presence of disturbances: Design, analysis and experiments. *Nonlinear Dyn.* **2024**, *112*, 7113–7127. [CrossRef]
39. Yang, M.; Wang, Z.; Yu, D.; Wang, Z.; Liu, Y.J. Extended state observer-based non-singular practical fixed-time adaptive consensus control of nonlinear multi-agent systems. *Nonlinear Dyn.* **2023**, *111*, 10097–10111. [CrossRef]
40. Fan, Y.; Qiu, B.; Liu, L.; Yang, Y. Global fixed-time trajectory tracking control of underactuated USV based on fixed-time extended state observer. *ISA Trans.* **2023**, *132*, 267–277. [CrossRef]
41. Deng, J.; Xue, W.; Zhang, L.; Bao, Q.; Mao, Y. Disturbance-Compression Extended State Observer with Noise Insensitivity: Application to Electro-Optical Tracking System. *IEEE Trans. Autom. Sci. Eng.* **2025**, *22*, 17761–17777. [CrossRef]
42. Zhai, J.; Li, S.; Xu, Z.; Zhang, L.; Li, J. Reduced-Order Extended State Observer-Based Sliding Mode Control for All-Clamped Plate Using an Inertial Actuator. *Energies* **2022**, *15*, 1780. [CrossRef]
43. Han, J.; Liu, X.; Wei, X.; Zhu, X. Reduced-Order Observer-Based Finite Time Fault Estimation for Switched Systems with Lager and Fast Time Varying Fault. *IEEE Trans. Circuits Syst. II Express Briefs* **2024**, *71*, 350–354. [CrossRef]
44. Li, S.; Kruszewski, A.; Guerra, T.M.; Nguyen, A.T. Equivalent-Input-Disturbance-Based Dynamic Tracking Control for Soft Robots via Reduced-Order Finite-Element Models. *IEEE/ASME Trans. Mechatron.* **2022**, *27*, 4078–4089. [CrossRef]
45. Wang, S.; Li, B.; Chen, P.; Yu, W.; Peng, Y.; Luo, Y. A fractional-order active disturbance rejection control for permanent magnet synchronous motor position servo system. *Asian J. Control* **2024**, *26*, 3137–3147. [CrossRef]
46. Zhao, M.; Hu, Y.; Song, J. Improved Fractional-Order Extended State Observer-Based Hypersonic Vehicle Active Disturbance Rejection Control. *Mathematics* **2022**, *10*, 4414. [CrossRef]
47. Zhao, J.; Zhao, T.; Liu, N.; Zhao, J.; Zhao, T.; Liu, N. Fractional-Order Active Disturbance Rejection Control with Fuzzy Self-Tuning for Precision Stabilized Platform. *Entropy* **2022**, *24*, 1681. [CrossRef]
48. Li, J.; Zhang, L.; Li, S.; Mao, Q.; Mao, Y. Active Disturbance Rejection Control for Piezoelectric Smart Structures: A Review. *Machines* **2023**, *11*, 174. [CrossRef]

49. Jiang, M.; Liu, J. Active Disturbance Rejection Control of Permanent Magnet Synchronous Motor Speed Control System Based On Improved Fal Function. In Proceedings of the 2024 5th International Conference on Mechatronics Technology and Intelligent Manufacturing, ICMTIM 2024, Nanjing, China, 26–28 April 2024; pp. 219–223. [CrossRef]
50. Xie, J.; Wei, W.; Liao, P.; Liu, J. Design of ADRC Controller for Induction Motor Based on Improved Fal Function. In Proceedings of the 2022 14th International Conference on Advanced Computational Intelligence, ICACI 2022, Wuhan, China, 15–17 July 2022; pp. 216–220. [CrossRef]
51. Zhu, L.; Zhang, G.; Jing, R.; Bi, G.; Xiang, R.; Wang, G.; Xu, D. Nonlinear Active Disturbance Rejection Control Strategy for Permanent Magnet Synchronous Motor Drives. *IEEE Trans. Energy Convers.* **2022**, *37*, 2119–2129. [CrossRef]
52. Jin, N.; Zhang, Y.; Lei, Y.; Sun, D. ADRC-IMC Strategy of PMSM Control System Based on Improved Fal Function. *Int. J. Electr. Hybrid Veh.* **2024**, *16*, 311–328. [CrossRef]
53. Yang, Z.; Ji, J.; Sun, X.; Zhu, H.; Zhao, Q. Active Disturbance Rejection Control for Bearingless Induction Motor Based on Hyperbolic Tangent Tracking Differentiator. *IEEE J. Emerg. Sel. Top. Power Electron.* **2020**, *8*, 2623–2633. [CrossRef]
54. Yang, S.; Ma, J.; Zhao, D.; Li, C.; Fang, L. Piecewise Sliding-Mode-Enhanced ADRC for Robust Active Disturbance Rejection Control Against Internal and Measurement Noise. *Sensors* **2025**, *25*, 6109. [CrossRef]
55. Zhang, D.; Wu, T.; Shi, S.; Dong, Z.; Zhang, D.; Wu, T.; Shi, S.; Dong, Z. A Modified Active-Disturbance-Rejection Control with Sliding Modes for an Uncertain System by Using a Novel Reaching Law. *Electronics* **2022**, *11*, 2392. [CrossRef]
56. Jiang, C.; Yin, C.; Gao, J.; Yuan, G. Position Control of Gear Shift based on Sliding Mode Active Disturbance Rejection Control for Small-Sized Tractors. *Sci. Prog.* **2022**, *105*, 00368504221081966. [CrossRef]
57. Zhang, T.; Jiao, X.; Lin, Z. Finite time trajectory tracking control of autonomous agricultural tractor integrated nonsingular fast terminal sliding mode and disturbance observer. *Biosyst. Eng.* **2022**, *219*, 153–164. [CrossRef]
58. Wang, Y.; Fang, S.; Hu, J. Active Disturbance Rejection Control Based on Deep Reinforcement Learning of PMSM for More Electric Aircraft. *IEEE Trans. Power Electron.* **2023**, *38*, 406–416. [CrossRef]
59. Zhao, Y.; Liu, C.; Liu, X.; Wang, H.; Zhou, Y. Adaptive tracking control for stochastic nonlinear systems with unknown virtual control coefficients. *Int. J. Robust Nonlinear Control* **2022**, *32*, 1331–1354. [CrossRef]
60. Seifullaev, R.; Knorn, S.; Ahlén, A. Event-triggered control of systems with sector-bounded nonlinearities and intermittent packet transmissions. *Automatica* **2022**, *146*, 110651. [CrossRef]
61. Ahmed, I.; Rehan, M.; Iqbal, N.; Ahn, C.K. A Novel Event-Triggered Consensus Approach for Generic Linear Multi-Agents Under Heterogeneous Sector-Restricted Input Nonlinearities. *IEEE Trans. Netw. Sci. Eng.* **2023**, *10*, 1648–1658. [CrossRef]


**Disclaimer/Publisher's Note:** The statements, opinions and data contained in all publications are solely those of the individual author(s) and contributor(s) and not of MDPI and/or the editor(s). MDPI and/or the editor(s) disclaim responsibility for any injury to people or property resulting from any ideas, methods, instructions or products referred to in the content.